

## REPORT No. 773

# ANALYSIS OF HEAT AND COMPRESSIBILITY EFFECTS IN INTERNAL FLOW SYSTEMS AND HIGH-SPEED TESTS OF A RAM-JET SYSTEM

By JOHN V. BECKER and DONALD D. BAALS

### SUMMARY

*An analysis has been made by the NACA of the effects of heat and compressibility in the flow through the internal systems of aircraft. Equations and charts are developed whereby the flow characteristics at key stations in a typical internal system may be readily obtained. The effects of compressibility (density change) were fully accounted for and were found to be important at present-day flight conditions, particularly at high altitudes. Particular attention was given to the flow changes across radiators and air-cooled engines. It is shown that very high Mach numbers will be attained within the fins of existing air-cooled engines if required cooling is to be maintained at altitude. The density decrease and the pressure drop across radiators and engines are shown to be considerably greater than the values computed on the basis of an incompressible flow. The equations show that when a Mach number of 1.0 is reached at any station of the internal system, the flow becomes choked and any further reduction of outlet pressure will not increase the flow rate. The addition of heat had a throttling effect on the flow rate and led to choking at lower rates of flow.*

*Tests of a 13-inch diameter ram-jet type of propulsion system using an electrical heating device to add heat to the internal flow have been made in the Langley 8-foot high-speed wind tunnel throughout a Mach number range of 0.2 to 0.75. The results showed that the measured thrusts and thermal efficiencies closely approached the ideal values for this type of propulsion system. Measurements of the flow details at various stations of the internal system were compared with calculations based on one-dimensional compressible flow theory, and excellent agreement was obtained.*

*In regard to the propulsive effect due to heating the internal flow, the thermal efficiency of the energy-recovery cycle was shown to depend mainly on the ratio of the static pressure in the duct behind the radiator to the stream static pressure. To a lesser extent, the thermal efficiency was governed by the Mach number of the duct flow and by the rate of heating; increases in either of these quantities caused decreases in the thermal efficiency.*

### INTRODUCTION

The operating speeds and the altitudes attained by modern aircraft have advanced to the point where the use of simple incompressible-flow relations in the design of internal ducts and cooling systems results in large errors in the determination of the internal-flow characteristics. A more

comprehensive analysis employing compressible-flow relations, therefore, is required in order to compute accurately the conditions at each station within the duct, the pressure drop across the radiator, the internal mass flow, and the variation of the internal-flow characteristics with the addition of heat. The effects of the addition of heat to the internal flow are also of importance because of the possibility of obtaining appreciable thrust power from the internal system.

References 1 and 2, which are representative of the numerous theoretical analyses comprising most of the previous work in this field, were concerned mainly with evaluating the net force resulting from the flow through the engine-cooling system. In these earlier analyses it was usually not necessary to compute the internal-flow characteristics in great detail and it was possible to neglect, in part, the effects of compressibility (density changes). A more comprehensive general discussion of the cooling-system air flow was given in reference 3 but the details of the flow relations involved were not shown.

In the present investigation a theoretical analysis of the flow details at key stations in a typical system was made. The effects of compressibility and of heating were accounted for up to Mach numbers of 1.0. Results of this analysis are presented in part I of the investigation in the form of charts and working equations that can be readily applied in practice.

Of great interest are the designs of internal flow systems that employ much higher rates of heating than are normally found in the cooling systems alone. The effectiveness of such designs depends on the thermal efficiency of the process whereby heat is converted into thrust power. For this reason, one of the principal purposes of this investigation was to study analytically the energy-recovery process and to determine by experiment how closely the ideal thermal efficiency could be approached in a typical system.

An experimental investigation of an idealized ram-jet propulsion system was conducted in the 8-foot high-speed wind tunnel at the Langley Memorial Aeronautical Laboratory in March 1941. The object of the present tests was to provide experimental data to establish the validity of the analytical results of part I, particularly with reference to the conversion of heat energy to thrust power. The results of these tests are presented in part II.

The body used in this investigation was designed to conform closely with the duct arrangement assumed in the analysis given in part I. Heat was added by a specially constructed radiator causing negligible blockage of the duct flow and insignificant friction loss. This manner of adding heat minimized the fire hazard in the wind tunnel and eliminated the combustion problem that would have existed if fuel were burned in the duct. The amount of heat added (160 kw max.) produced a thrust equal to about 40 percent of the drag of the test body at  $M=0.75$ . This rate of heating, although lower than the rates obtainable by combustion of fuel, was large enough to permit accurate measurements of the thrust and other effects of heating to be obtained and thus to provide the basis for significant comparisons with the analytical investigation.

## SYMBOLS

|              |   |
|--------------|---|
| $A$          | area, square feet   |
| $a$          | velocity of sound, feet per second  |
| $C$          | mass-flow coefficient $\left(\frac{m}{\rho_0 F V_0}\right)$ or $\left(\frac{A_0}{F}\right)$ |
| $C_D$        | internal-drag coefficient $\left(\frac{D}{q_0 F}\right)$                                    |
| $\Delta C_D$ | internal-drag-coefficient increment $\left(\frac{\Delta D}{q_0 F}\right)$                   |
| $C_{D_f}$    | drag coefficient of radiator tube $\left(\frac{D_f}{q_2 A_{r_2}}\right)$                    |
| $C_{D_r}$    | radiator drag coefficient $\left(\frac{D_r}{q_2 A_2}\right)$                                |
| $c_p$        | specific heat at constant pressure (for air 0.24 Btu/lb/°F)                                 |
| $D$          | net drag due to internal flow, pounds   |
| $\Delta D$   | internal-drag increment, pounds   |
| $D_f$        | drag force due to friction within the radiator tubes, pounds                                |
| $D_r$        | total drag force acting on the radiator, pounds   |
| $d$          | duct diameter, inches   |
| $F$          | maximum fuselage cross-section area, square feet (1.009 for model tested)                   |
| $g$          | acceleration of gravity (32.2 ft/sec <sup>2</sup> )   |
| $H$          | heat added, Btu per second  |
| $h$          | total pressure, pounds per square foot absolute   |
| $\Delta h$   | total-pressure loss, pounds per square foot   |
| $J$          | mechanical equivalent of heat (778 ft-lb/Btu)   |
| $K. E.$      | kinetic energy, foot-pounds   |
| $L$          | over-all length of fuselage, inches   |
| $l$          | distance from nose, inches  |
| $M$          | Mach number ( $v/a$ )   |
| $m$          | mass-flow rate, slugs per second  |
| $P$          | pressure coefficient $\left(\frac{p-p_0}{q_0}\right)$                                       |
| $p$          | static pressure, pounds per square foot absolute  |
| $\Delta p$   | static-pressure decrease, pounds per square foot  |
| $Q$          | quantity of flow, cubic feet per second   |
| $q$          | dynamic pressure, pounds per square foot $\left(\frac{1}{2}\rho V^2\right)$                 |
| $R$          | gas constant, feet per °F (for air, 53.3)   |
| $R$          | radius, inches  |

|              |   |
|--------------|---|
| $T$          | temperature, °F absolute  |
| $T$          | thrust, pounds  |
| $\Delta t$   | temperature change, °F  |
| $V_0$        | free-stream velocity, feet per second                             |
| $v$          | velocity within duct, feet per second                             |
| $x$          | distance from leading edge of respective sections, inches         |
| $\gamma$     | ratio of specific heats (for air, 1.40)                           |
| $\epsilon_H$ | heat-cycle efficiency (equation (31))                             |
| $\epsilon_M$ | mechanical-efficiency factor (equation (33))                      |
| $\epsilon_P$ | propulsive efficiency ( $\epsilon_H \epsilon_M$ ) (equation (32)) |
| $\rho$       | density, slugs per cubic foot                                     |
| $\eta_d$     | diffuser efficiency   |
| $1+\eta$     | compressibility factor  |

$$\left(\frac{h-p}{q} = 1 + \frac{M^2}{4} + \frac{M^4}{40} + \frac{M^6}{1600} \dots\right)$$

## Subscripts:

|        |  |
|--------|--|
| 0 to 5 | stations in internal flow system shown in figure 1 |
| $c$    | test condition without heat                        |
| $d$    | value at any station in duct                       |
| $f$    | friction component                                 |
| $i$    | low speed, incompressible-flow condition           |
| $r$    | condition across the radiator or heating device    |
| $r_2$  | within the radiator at the tube entrances          |
| $r_3$  | within the radiator at the tube exits              |
| $t$    | condition within the radiator tubes                |

A prime after a symbol indicates the condition without heat but with same mass flow as with heat.

## I. ANALYSIS OF INTERNAL FLOW SYSTEMS

## CALCULATION OF THE FLOW CHARACTERISTICS AT KEY STATIONS IN A TYPICAL INTERNAL FLOW SYSTEM

In the design of efficient aircraft, the flow characteristics (static pressure, density, and velocity) must be computed at several key stations in each internal flow system. The objects of such calculations are to determine the state of the air entering the radiators, the pressures available for cooling, the flow changes across the heating device, the net drag or propulsive force due to the internal flow, and the required sizes of inlet and outlet openings. It will be shown that under present-day operating conditions compressibility effects and the secondary effects of heating cannot be neglected in the calculations.

Methods will be presented for analyzing the internal flow system that will account for the effects of heating and compressibility and will yet be simple to use. Elimination of much of the mathematical work will be effected through solution of the more cumbersome equations in chart form. The methods presented are generally applicable to any internal flow system, either with or without the addition of heat or mechanical energy (internal blower), and for any rate of internal flow.

One-dimensional flow and a uniform velocity distribution across the duct is assumed throughout the analysis.

The theory of the process whereby the heat energy added to the internal flow is converted into mechanical energy is described under a subsequent subheading of part I.

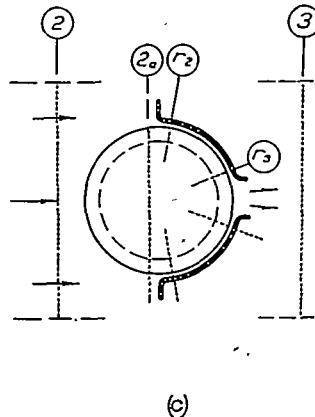
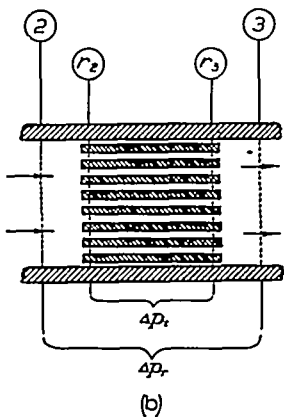
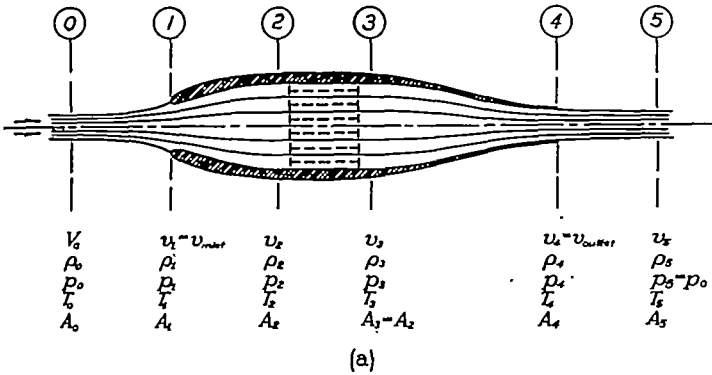
**Initial conditions.**—The initial quantities assumed to be known by the designer are as follows:

- (1) The rate at which heat is to be dissipated  $H$ , Btu per second
- (2) The pressure drop for the cold radiator  $(\Delta p/q_2)$ , obtained from low-speed tests
- (3) The mass-flow rate required by the system  $m$ , slugs per second
- (4) The speed of flight  $V_0$  and the atmospheric conditions  $p_0$ ,  $\rho_0$ , and  $T_0$
- (5) The duct areas available at all stations in the internal system

**Station 0.**—In the method to be described, the internal flow is considered as a stream tube starting far ahead of the airplane where the velocity in the tube (relative to the airplane) is  $V_0$  and the air conditions are those of the free stream (fig. 1). The area of the tube at this station is determined by the required rate of internal flow; that is,

$$A_0 = \frac{m}{\rho_0 V_0} \quad (1)$$

The area  $A_0$  is noted to be a measure of the mass flow and bears a simple relation to the flow coefficients,  $\frac{Q}{FV_0}$  and  $\frac{m}{\rho_0 FV_0}$ .



(a) For internal-flow analysis.

(b) For tubular radiator.

(c) For baffled air-cooled cylinder.

FIGURE 1.—Station designation.

If  $Q$  equals the volume rate of flow at any station  $d$ , then

$$\frac{Q}{FV_0} = \frac{m}{\rho_d FV_0} = \frac{\rho_0 A_0}{\rho_d F}$$

The mass-flow coefficient  $C$  is

$$C = \frac{m}{\rho_0 FV_0} = \frac{A_0}{F}$$

For isentropic flow, the pressure, the density, and the temperature at any station in the duct for any rate of internal flow can be related to the known initial conditions through the area ratio  $A_0/A_d$  and the Mach number  $M_0 = \frac{V_0}{a_0}$ , where  $a_0 = 49.0\sqrt{T_0}$ . Charts for obtaining these desired characteristics for known values of the area ratio and Mach number are given as figure 2 (pressure), figure 3 (density), and figure 4 (temperature).

The mathematical basis for these curves was derived as follows: By Bernoulli's equation for adiabatic compressible flow,

$$\frac{V_0^2}{2} + \frac{\gamma}{\gamma-1} \frac{p_0}{\rho_0} = \frac{v_d^2}{2} + \frac{\gamma}{\gamma-1} \frac{p_d}{\rho_d} \quad (2)$$

From the requirement of flow continuity,

$$\rho_0 A_0 V_0 = \rho_d A_d v_d$$

whence

$$v_d^2 = V_0^2 \left(\frac{\rho_0}{\rho_d}\right)^2 \left(\frac{A_0}{A_d}\right)^2$$

Also,

$$M_0^2 = \frac{\rho_0 V_0^2}{\gamma p_0}$$

and for isentropic flow

$$\left(\frac{\rho_0}{\rho_d}\right)^2 = \left(\frac{p_0}{p_d}\right)^{2/\gamma}$$

By substitution of these relations into equation (2) in order to eliminate the velocity and density terms, the following result is obtained:

$$\frac{\gamma-1}{2} M_0^2 \left(\frac{A_0}{A_d}\right)^2 \left(\frac{p_d}{p_0}\right)^{-2/\gamma} + \left(\frac{p_d}{p_0}\right)^{\frac{\gamma-1}{\gamma}} = \frac{\gamma-1}{2} M_0^2 + 1 \quad (3)$$

This equation is solved in figure 2 for  $p_d/p_0$  in terms of  $M_0$  and  $A_0/A_d$ . The density and temperature ratios in the duct can be computed from the pressure-ratio values obtained from equation (3). For isentropic flow

$$\frac{\rho_d}{\rho_0} = \left(\frac{p_d}{p_0}\right)^{1/\gamma}$$

and

$$\frac{T_d}{T_0} = \left(\frac{p_d}{p_0}\right)^{\frac{\gamma-1}{\gamma}}$$

The use of figures 3 and 4 permits the density and temperature ratios to be obtained directly for the known values of  $M_0$  and  $A_0/A_d$ .

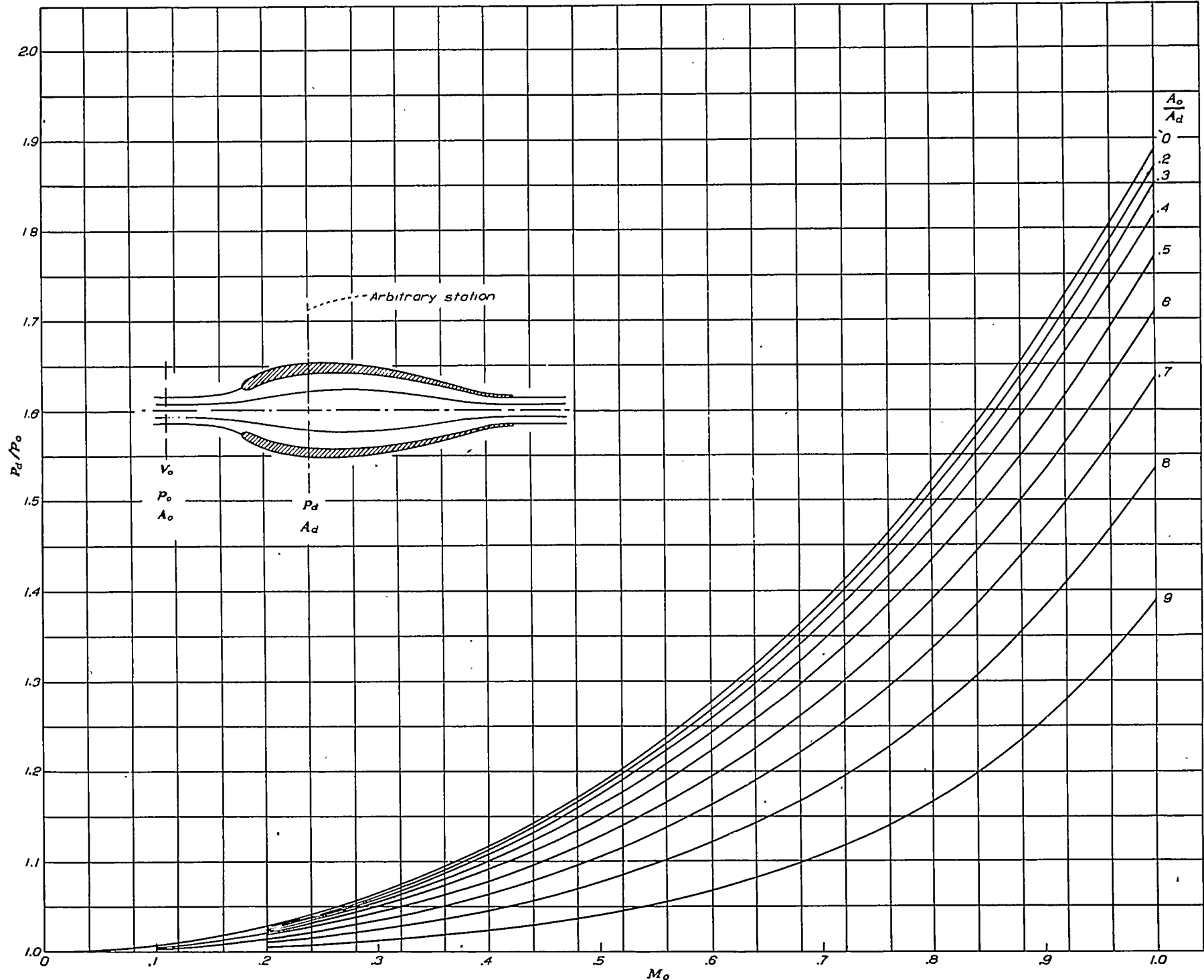


FIGURE 2.—Variation of pressure ratio with area ratio for a given Mach number. Diffuser efficiency=1.0.

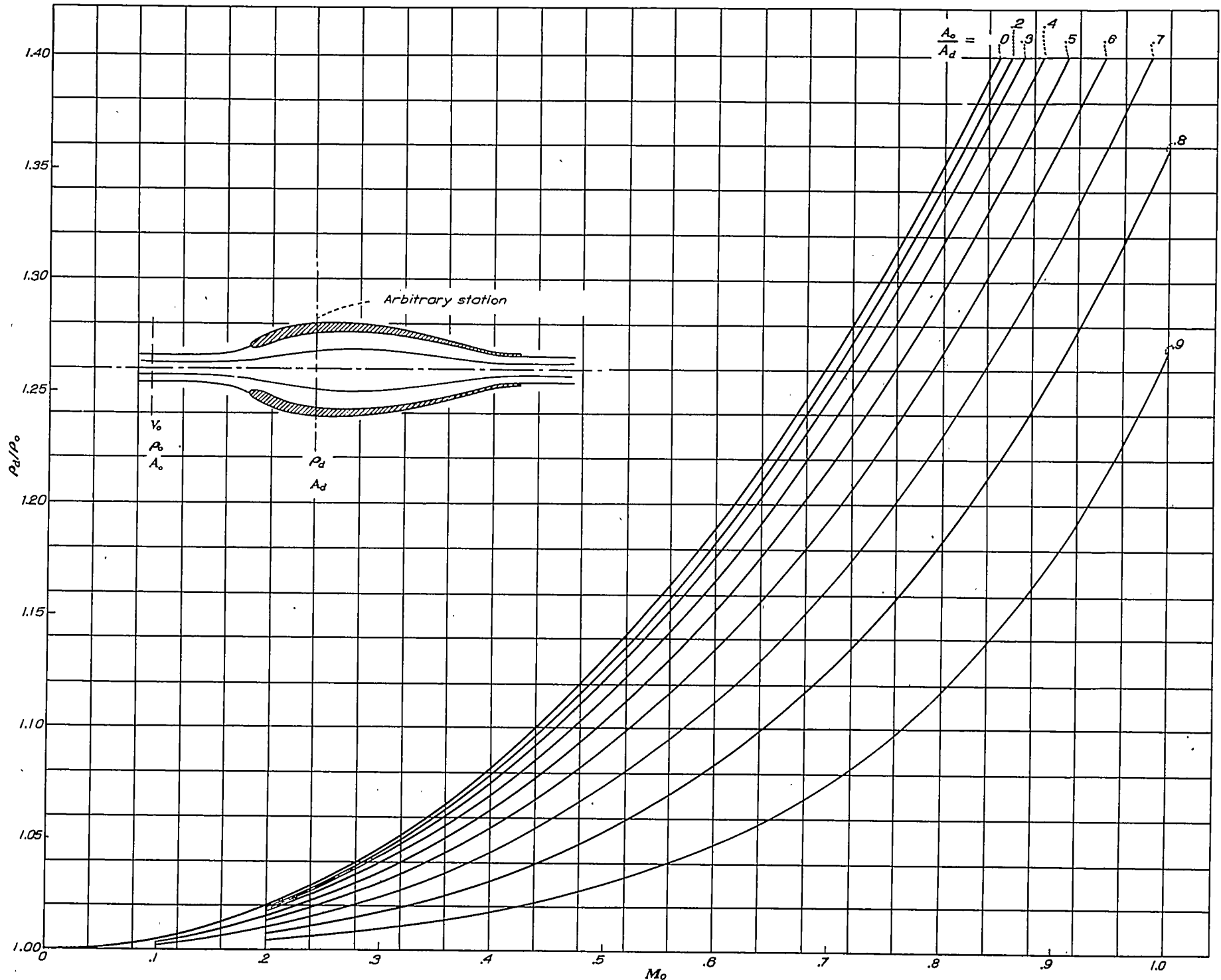


FIGURE 3.—Variation of density ratio with area ratio for a given Mach number. Diffuser efficiency=1.0.

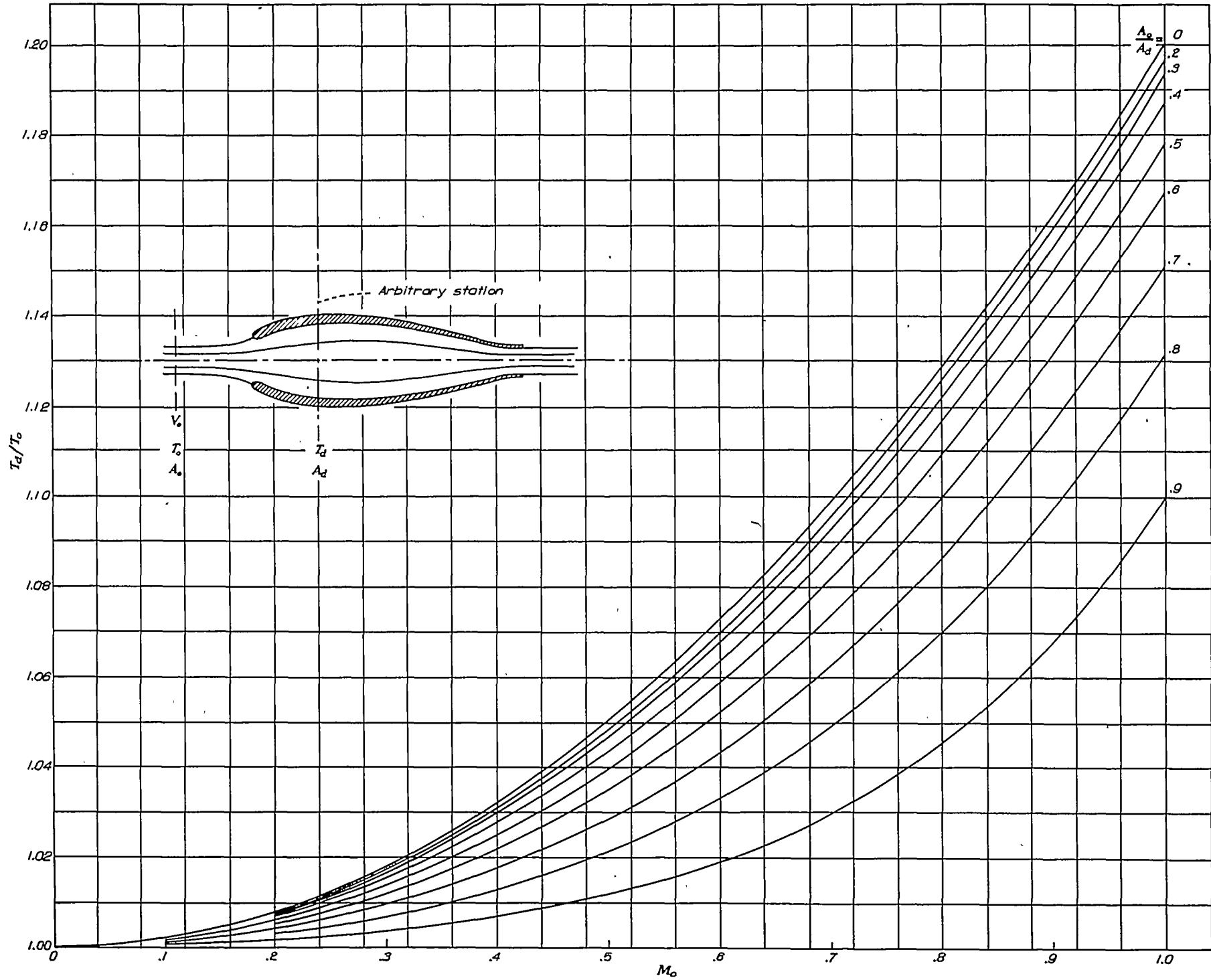


FIGURE 4.—Variation of temperature ratio with area ratio of a given Mach number. Diffuser efficiency=1.0.

The use of the charts (figs. 2, 3, and 4) is not restricted to the Mach number  $M_0$  and the area ratio  $A_0/A_d$ , as indicated by the subscripts on the figures. For example, if the area ratio and Mach number were taken as  $A_1/A_d$  and  $M_1$  respectively, the charts would yield the ratios  $p_1/p_d$ ,  $\rho_1/\rho_d$ , and  $T_1/T_d$ . Any other more convenient area and corresponding Mach number might be similarly used in place of  $A_0$  and  $M_0$ . The charts may also be employed to determine the flow from a large area to a small area. The Mach number used with the charts must always be the Mach number corresponding to the smaller area.

**Station 1.**—The entrance area  $A_1$  should be designed to allow the desired mass flow to enter the duct at an inlet-velocity ratio that will permit efficient external flow as well as efficient internal flow. In the investigation reported in reference 4, velocity ratios of 0.3 to 0.6 were found to fulfill these requirements for circular openings of suitable shape located at the stagnation point of a body. Higher inlet-velocity ratios will make it difficult to expand the internal flow efficiently, and lower inlet-velocity ratios will generally make the external flow unsatisfactory for high-speed airplanes. If the inlet-velocity  $v_1$  is selected on the basis of these considerations, the inlet area is given by

$$A_1 = \frac{m}{\rho_1 v_1} \quad (4)$$

In most applications a sufficiently accurate value of  $A_1$  will be obtained when  $\rho_1$  is taken as equal to  $\rho_0$ .

After the entrance area and the ratio  $A_0/A_1$  have been determined, the pressure, the density, and the temperature at station 1 may be obtained directly from the charts if the opening is not located within a boundary layer.

**Station 2.**—If the ducting losses between stations 1 and 2 are a negligible fraction of the free-stream dynamic pressure, the static pressure, the density, and the temperature at station 2 may be obtained directly from the charts (figs. 2, 3, and 4) for the area ratio  $A_0/A_2$ .

Under most conditions of flight, however, it will be necessary to account for the diffuser losses even in efficient systems. The characteristics of the diffuser are usually defined by a diffuser efficiency,

$$\eta_d = \left( \frac{p_2 - p_1}{q_1 - q_2} \right)_d$$

or, preferably,

$$\eta_d = 1 - \frac{\Delta h_2}{q_1 - q_2}$$

The definition in terms of the static pressures, as indicated, can be used only in the reduction of incompressible-flow data because, at high speeds, the pressure rise is affected by factors other than the diffuser shape. The definition in terms of the total-pressure loss between stations 1 and 2, however, which yields the same value for  $\eta_d$  at low speeds, remains essentially constant with Mach number (see reference 5) and should therefore be used for all high-speed test data. If the velocity distribution is reasonably uniform, the total-pressure loss in the diffuser will equal the decrease in static pressure at station 2 below the ideal static pressure for zero friction loss; that is,

$$\Delta p_2 = \Delta h_2 = (q_1 - q_2)(1 - \eta_d) = q_1 \left[ 1 - \left( \frac{A_1}{A_2} \right)^2 \right] (1 - \eta_d)$$

The assumption of incompressible flow in computing the local dynamic-pressure ratio is justified in the usual case where the Mach number at the entrance is low and where  $\Delta h_2$  is small.

The static-pressure ratio at station 2 is therefore

$$\frac{p_2}{p_0} = \left( \frac{p_2}{p_0} \right)_{ideal} - \frac{q_1}{p_0} \left[ 1 - \left( \frac{A_1}{A_2} \right)^2 \right] (1 - \eta_d) \quad (5)$$

The ideal pressure ratio is obtained as before from figure 2, and the diffuser efficiency  $\eta_d$  can be estimated from test data such as that given in references 5 and 6. Data on the diffuser efficiency for the model used in the present tests are given in reference 5.

The temperature distribution across the duct at station 2 is not uniform, the temperature being slightly higher near the walls where the friction effects predominate. A satisfactory value is given by

$$\frac{T_2}{T_0} = \left( \frac{p_2}{p_0} \right)_{ideal}^{\frac{\gamma-1}{\gamma}} = \left( \frac{p_2}{p_0} \right)_{ideal}^{0.286}$$

in which the ideal pressure ratio of figure 2 is used. The corresponding value of the density is

$$\rho_2 = \frac{p_2}{gRT_2} = 0.000583 \frac{p_2}{T_2}$$

The Mach number of the flow in the duct at station 2 will be shown to be an important parameter and is given by

$$M_2 = M_0 \frac{v_2}{V_0} \frac{a_0}{a_2} = M_0 \frac{\rho_0}{\rho_2} \frac{A_0}{A_2} \left( \frac{T_0}{T_2} \right)^{1/2}$$

**Flow changes within the radiator.**—An exact determination of the flow changes between stations 2 and 3 must include calculations of the flow details within the heating device. The following analysis describes the flow through a tube or channel of constant cross section in which heat is added and in which friction losses occur.

If no appreciable energy losses are assumed to occur at the tube entrances, it is apparent that the flow changes between station 2 and station  $r_2$  (at the tube entrance) are determined by the area ratio  $A_{r_2}/A_2$  and the Mach number  $M_{r_2}$ , where  $A_{r_2}$  is the free area within the radiator. Figures 2, 3, and 4 may therefore be used to obtain the desired conditions at station  $r_2$  by merely changing the nomenclature on these charts. The charts require the use of the Mach number  $M_{r_2}$ , which may be computed from the known value of  $M_2$  as follows:

$$M_{r_2} = M_2 \frac{A_2}{A_{r_2}} \frac{\rho_2}{\rho_{r_2}} \left( \frac{T_2}{T_{r_2}} \right)^{1/2}$$

The value of  $M_{r_2}$  is dependent on  $\rho_2/\rho_{r_2}$  and  $T_2/T_{r_2}$ , values which are to be obtained from the charts. A trial and error process must therefore be employed until corresponding values of  $M_{r_2}$ ,  $\rho_2/\rho_{r_2}$ , and  $T_2/T_{r_2}$  are obtained. Two or three

trials usually suffice. The pressure drop of the air entering the tube is given by

$$p_2 - p_{r_2} = p_2 \left( 1 - \frac{p_{r_2}}{p_2} \right) \quad (6)$$

in which  $p_2/p_{r_2}$  is obtained directly from figure 2, for the value of  $A_{r_2}/A_2$  and  $M_{r_2}$  as just described.

The pressure drop between stations  $r_2$  and  $r_3$  (at the tube entrance and exit) is obtained by applying the momentum relation between these stations:

$$p_{r_2} + \rho_{r_2} v_{r_2}^2 = p_{r_3} + \rho_{r_3} v_{r_3}^2 + \frac{D_f}{A_{r_2}}$$

where  $D_f$  is the drag force due to friction within the radiator tubes and  $A_{r_2} = A_{r_3}$ . The pressure drop in terms of  $q_{r_2}$  is, thus,

$$\frac{\Delta p_t}{q_{r_2}} = \frac{p_{r_2} - p_{r_3}}{q_{r_2}} = \frac{D_f}{q_{r_2} A_{r_2}} + \frac{\rho_{r_3} v_{r_3}^2 - \rho_{r_2} v_{r_2}^2}{q_{r_2}} \quad (7)$$

It is evident from equation (7) that the pressure drop in the tube is comprised of two components: First, a pressure drop associated with the frictional drag force and, second, a pressure drop due to the momentum increase in the tube. This second term, frequently neglected, becomes very important when the velocity in the tube is large. The drag term is presented in the form of a drag coefficient, denoted hereinafter as  $C_{D_f}$ , where

$$C_{D_f} = \frac{D_f}{q_{r_2} A_{r_2}}$$

The basic value of  $C_{D_f}$  corresponding to the unheated low-speed condition  $C_{D_{f_t}}$  can be determined from pressure-drop measurements for this condition:

$$C_{D_{f_t}} = \left( \frac{D_f}{q_{r_2} A_{r_2}} \right)_t = \left( \frac{\Delta p_f A_{r_2}}{q_{r_2} A_{r_2}} \right)_t = \left( \frac{\Delta p_f}{q_{r_2}} \right)_t$$

This basic value of the drag coefficient depends on the geometry of the radiator tubes and on the Reynolds number. A considerable volume of pressure-drop data for radiator tubes is available and may be used to compute  $C_{D_{f_t}}$ . When heat is applied, the drag coefficient increases because of the increase in dynamic pressure along the tube. If this drag increase is assumed to be proportional to the mean dynamic pressure in the tube,

$$C_{D_f} = C_{D_{f_t}} \left[ \frac{1}{2} \left( 1 + \frac{\rho_{r_2}}{\rho_{r_3}} \right) \right] \quad (8)$$

or

$$\frac{\Delta p_f}{q_{r_2}} = \left( \frac{\Delta p_f}{q_{r_2}} \right)_t \left[ \frac{1}{2} \left( 1 + \frac{\rho_{r_2}}{\rho_{r_3}} \right) \right]$$

In order to evaluate  $C_{D_f}$  from the known basic value  $C_{D_{f_t}}$ , the density ratio  $\rho_{r_2}/\rho_{r_3}$  must be obtained. This relation is also required in evaluating  $\Delta p_t/q_{r_2}$  (equation (7)). A method for computing  $\rho_{r_2}/\rho_{r_3}$  exactly will now be described.

The density ratio will be obtained by solving simultaneously the momentum, energy, and continuity relations between the flows at stations  $r_2$  and  $r_3$ . Equation (7) shows the momentum relation. The energy equation, relating the total energy per unit mass at the two stations, is

$$\frac{v_{r_2}^2}{2} + \frac{\gamma}{\gamma-1} \frac{p_{r_2}}{\rho_{r_2}} + \frac{JH}{m} = \frac{v_{r_3}^2}{2} + \frac{\gamma}{\gamma-1} \frac{p_{r_3}}{\rho_{r_3}} \quad (9)$$

Since the areas at stations  $r_2$  and  $r_3$  are equal,

$$\rho_{r_2} v_{r_2} = \rho_{r_3} v_{r_3}$$

Solving the last three equations simultaneously for  $\rho_{r_2}/\rho_{r_3}$  gives

$$\frac{\rho_{r_2}}{\rho_{r_3}} = 1 + \frac{H}{c_p g m T_{r_2}} + 0.2 M_{r_2}^2 \left[ 1 - \left( \frac{\rho_{r_2}}{\rho_{r_3}} \right)^2 + 7.0 \frac{\rho_{r_2}}{\rho_{r_3}} \left( \frac{C_{D_f}}{2} + \frac{\rho_{r_2}}{\rho_{r_3}} - 1 \right) \right] \quad (10)$$

This relation has been evaluated for a wide range of values of heat input and radiator drag coefficients and the results are given in figure 5 for use in design and performance work. Values of  $\rho_{r_2}/\rho_{r_3}$  obtained from figure 5 with an estimated  $C_{D_f}$  may be substituted in equation (8) to obtain a more exact value of  $C_{D_f}$ . This process may then be repeated until the correct values of  $\rho_{r_2}/\rho_{r_3}$  and  $C_{D_f}$  are obtained. Two or three trials are usually sufficient.

Several interesting conclusions may be drawn from a study of equation (10) or figure 5. When the Mach number  $M_{r_2}$  of the flow approaches zero, the value of  $\rho_{r_2}/\rho_{r_3}$  approaches  $1 + \frac{H}{c_p g m T_{r_2}}$  or  $1 + \frac{T_{r_3} - T_{r_2}}{T_{r_2}}$ , the density ratio for heating at constant pressure. As  $M_{r_2}$  becomes greater, the pressure drop rapidly increases, with the result that the density ratio  $\rho_{r_2}/\rho_{r_3}$  increases above the constant-pressure value  $1 + \frac{H}{c_p g m T_{r_2}}$ .

This effect is very great for large values of  $M_{r_2}$ , such as are encountered with air-cooled engines.

For each radiator drag coefficient a limiting value of  $M_{r_2}$  is reached beyond which the solution of equation (10) becomes imaginary. This limiting condition occurs when the flow velocity at the tube outlets reaches the speed of sound, that is, when  $M_{r_3} = 1.0$ . A curve connecting the limiting density ratios is shown in figure 5. When the drag coefficients or the rate of heating is high, this critical condition is reached at low values of  $M_{r_2}$ , owing to the large density decrease along the tube. No increase in mass flow can occur after this critical condition has been reached. It may be inferred from the general knowledge of nozzles that shock waves will occur at the tube exits if the pressure drop is increased after sonic velocity has been reached. The energy corresponding to the increased pressure drop is dissipated in these shock waves and no increase in mass-flow rate occurs. The use of figure 5 as outlined will automatically indicate when this limiting condition is reached.

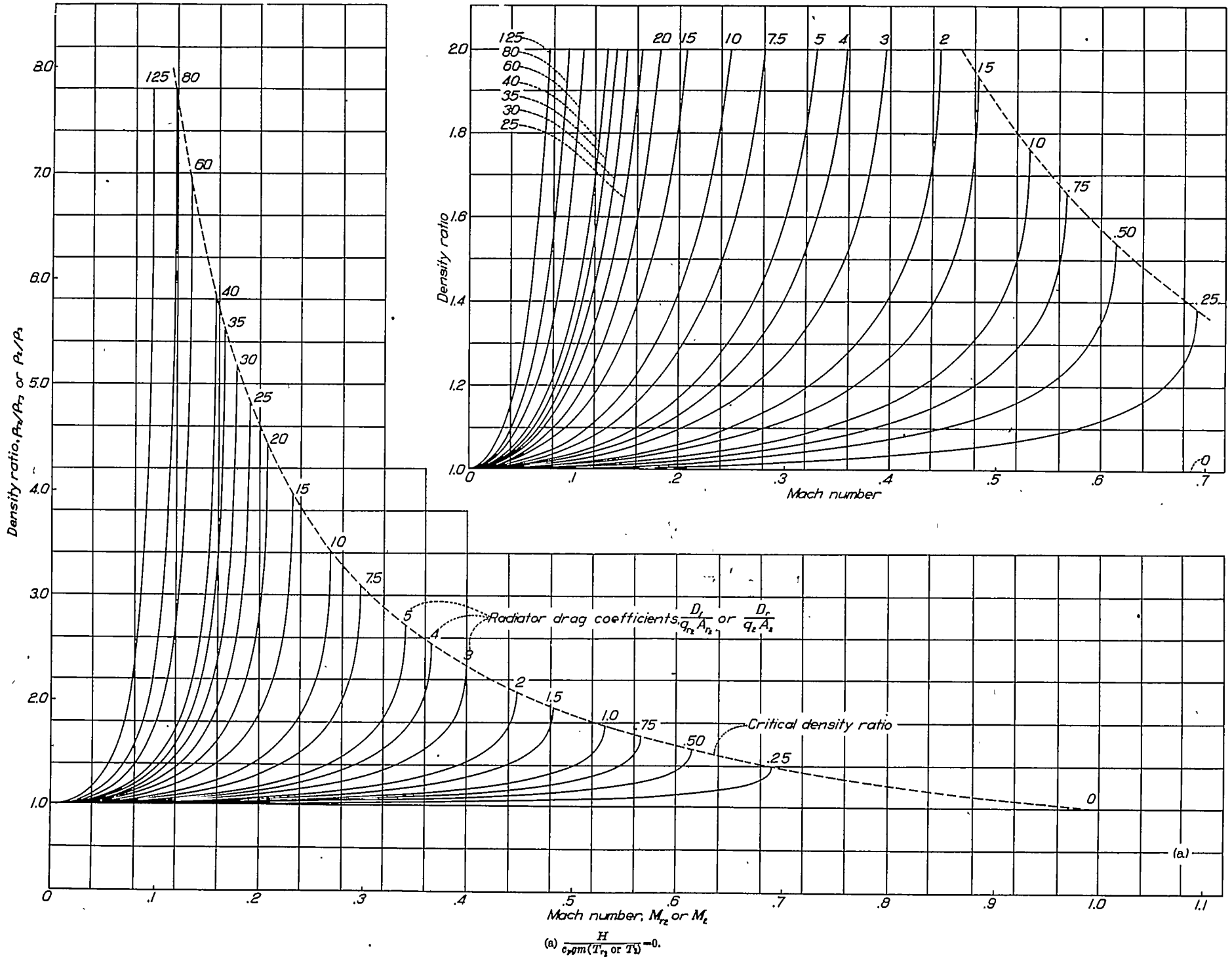
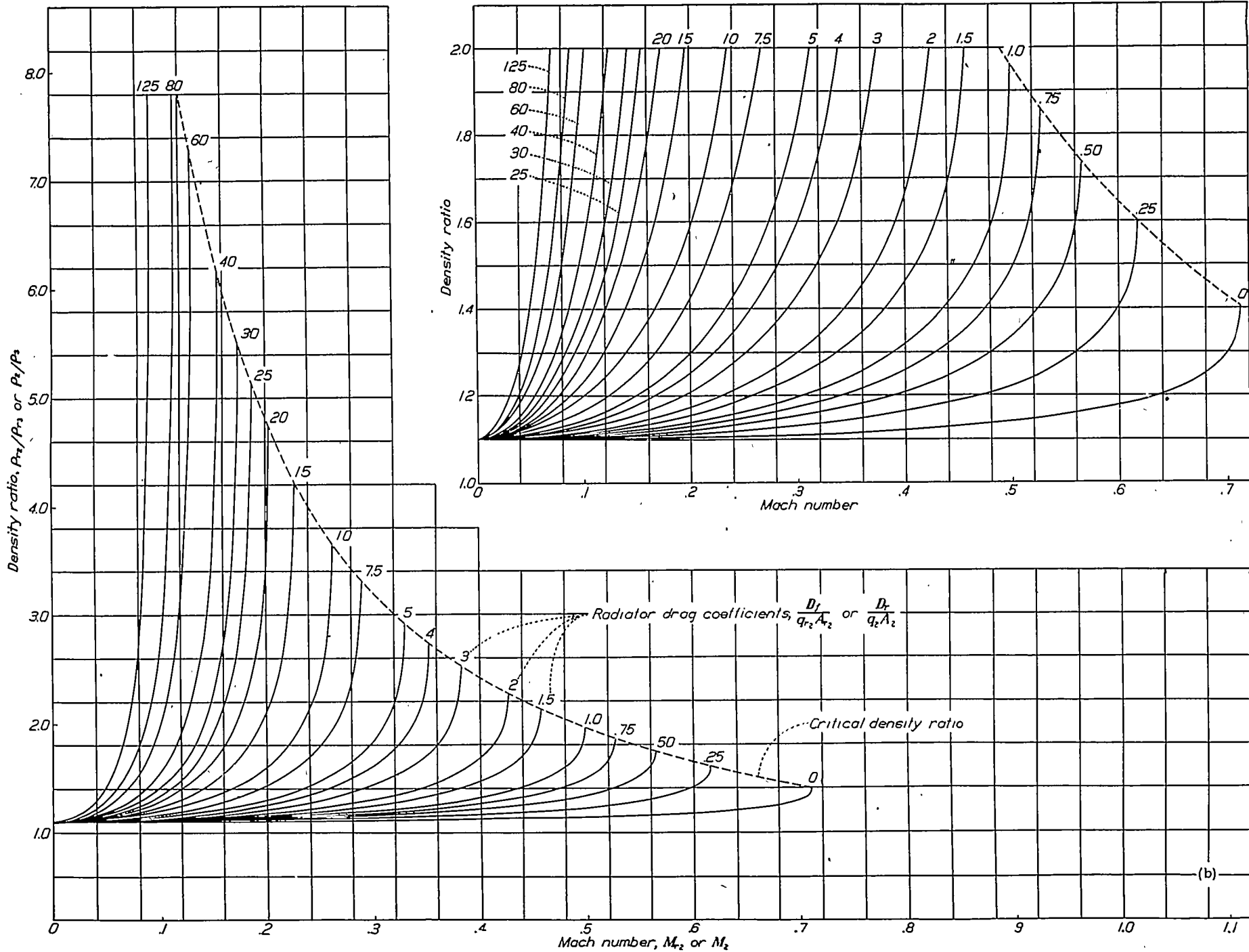
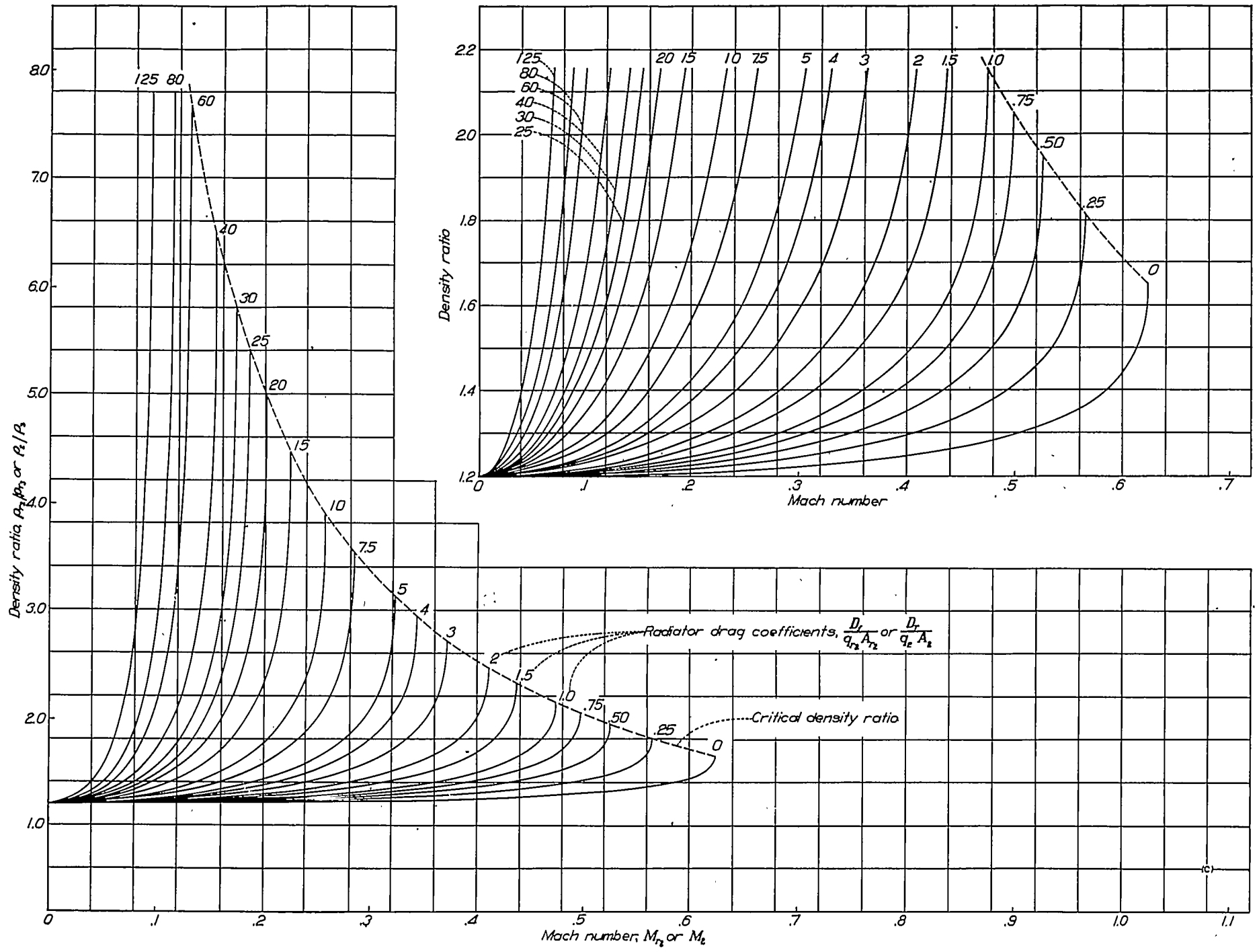


FIGURE 5.—Curves for obtaining density ratio across radiator.



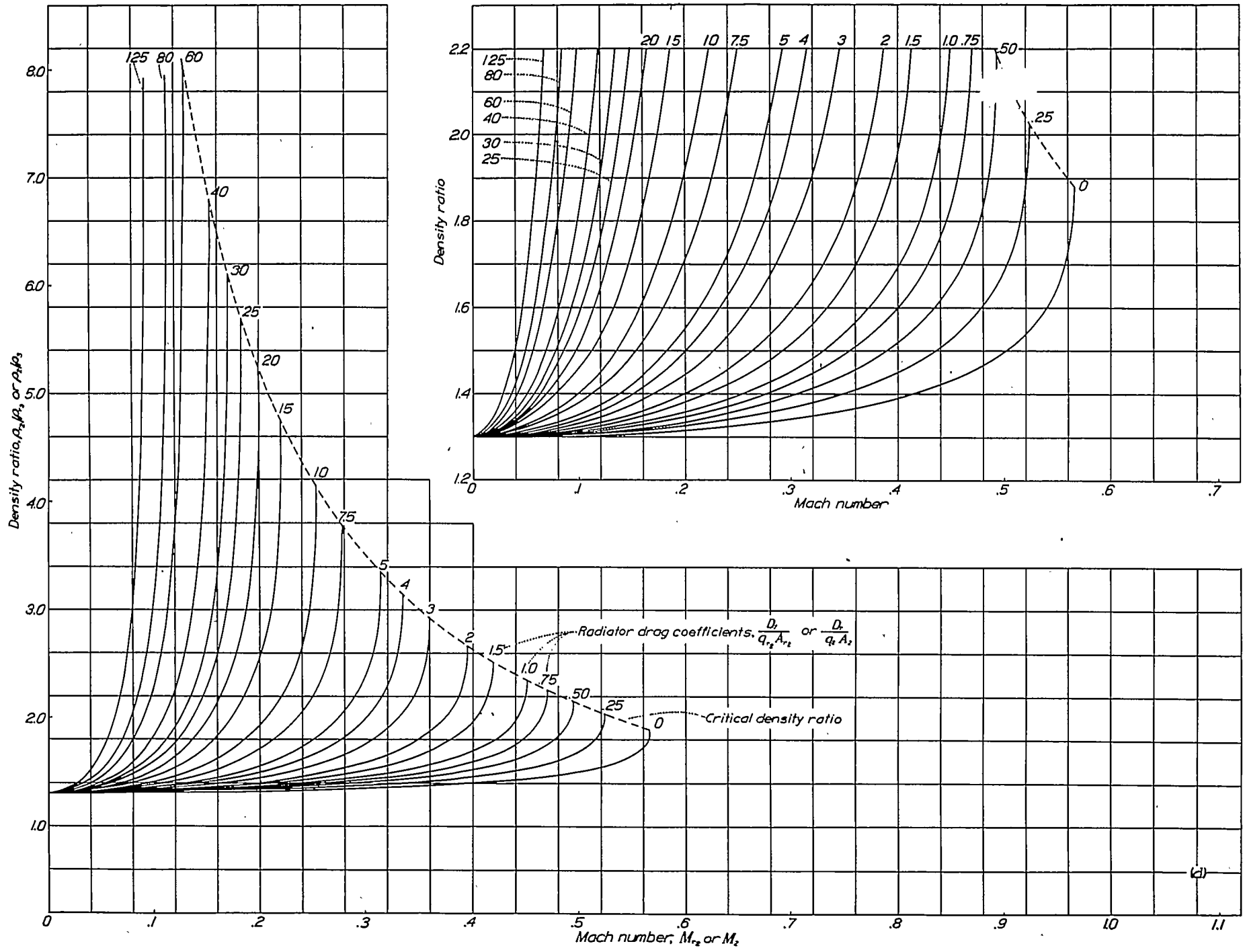
(b)  $\frac{H}{c_p \gamma m (T_{r_2} \text{ or } T_1)} = 0.1.$

FIGURE 5.—Continued.



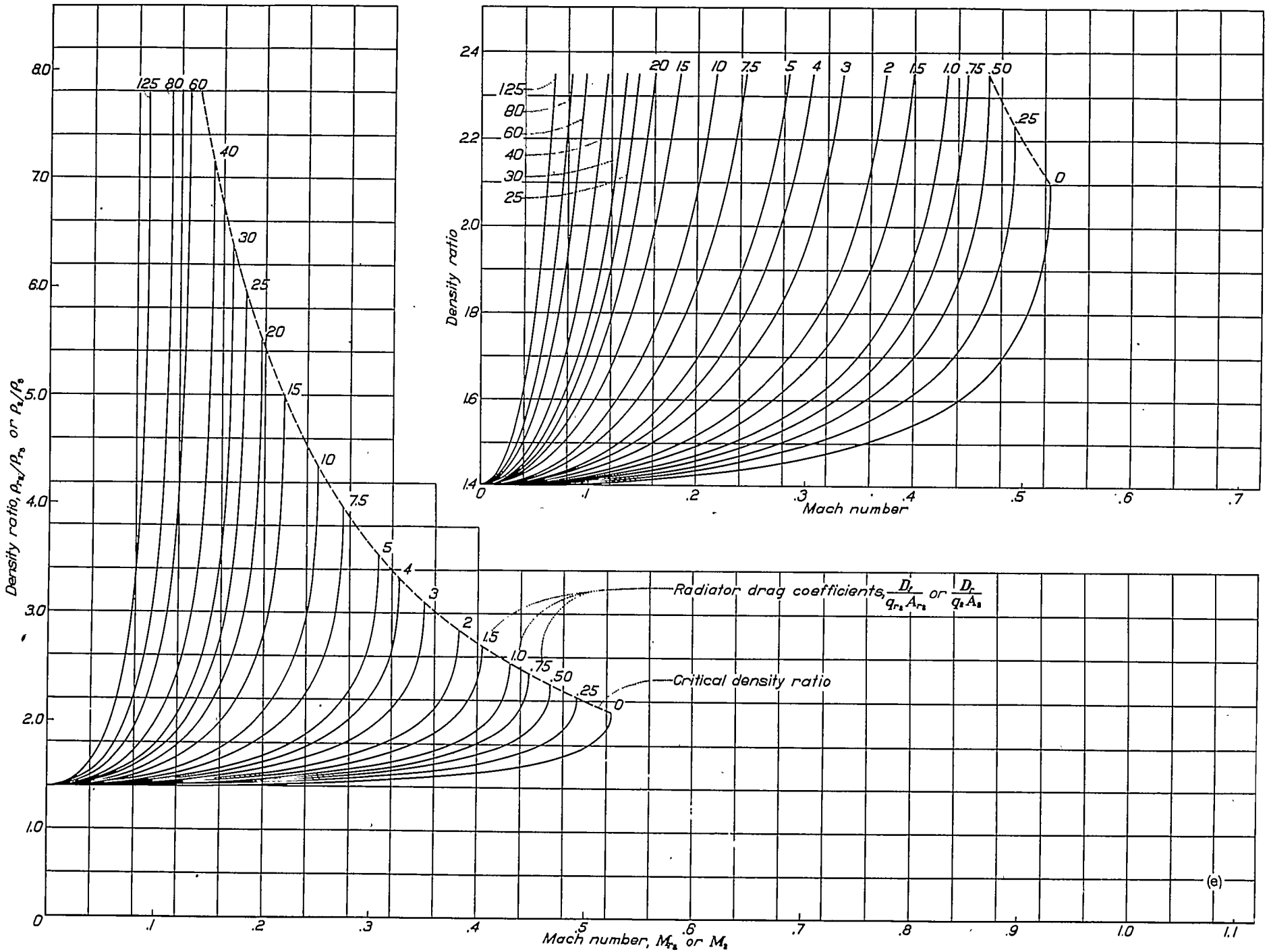
(c)  $\frac{F_1}{c_p g m (T_{r2} \text{ or } T_2)} = 0.2$

FIGURE 6.—Continued.



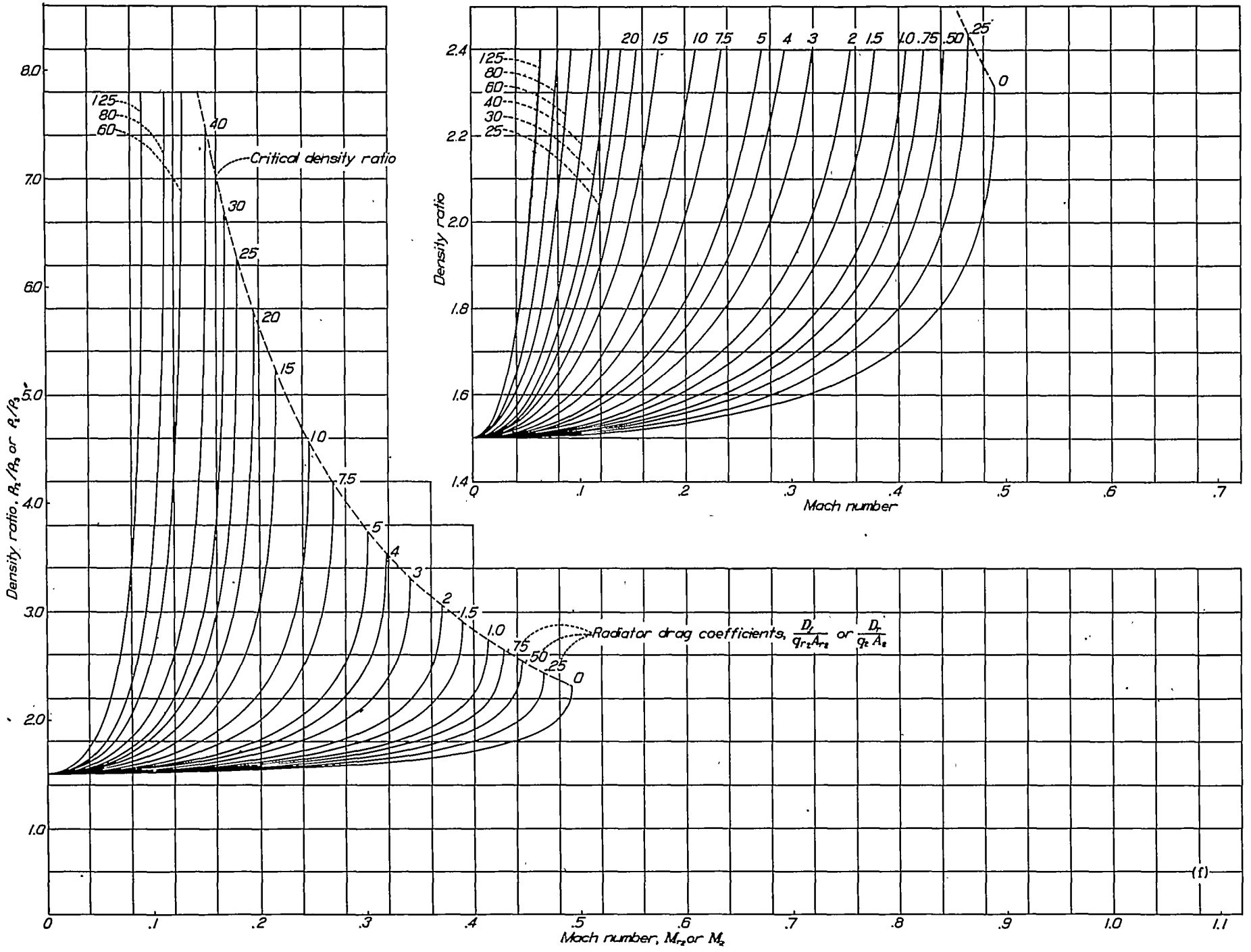
(d)  $\frac{H}{c_p g m (T_{r2} \text{ or } T_2)} = 0.3.$

FIGURE 5.—Continued.



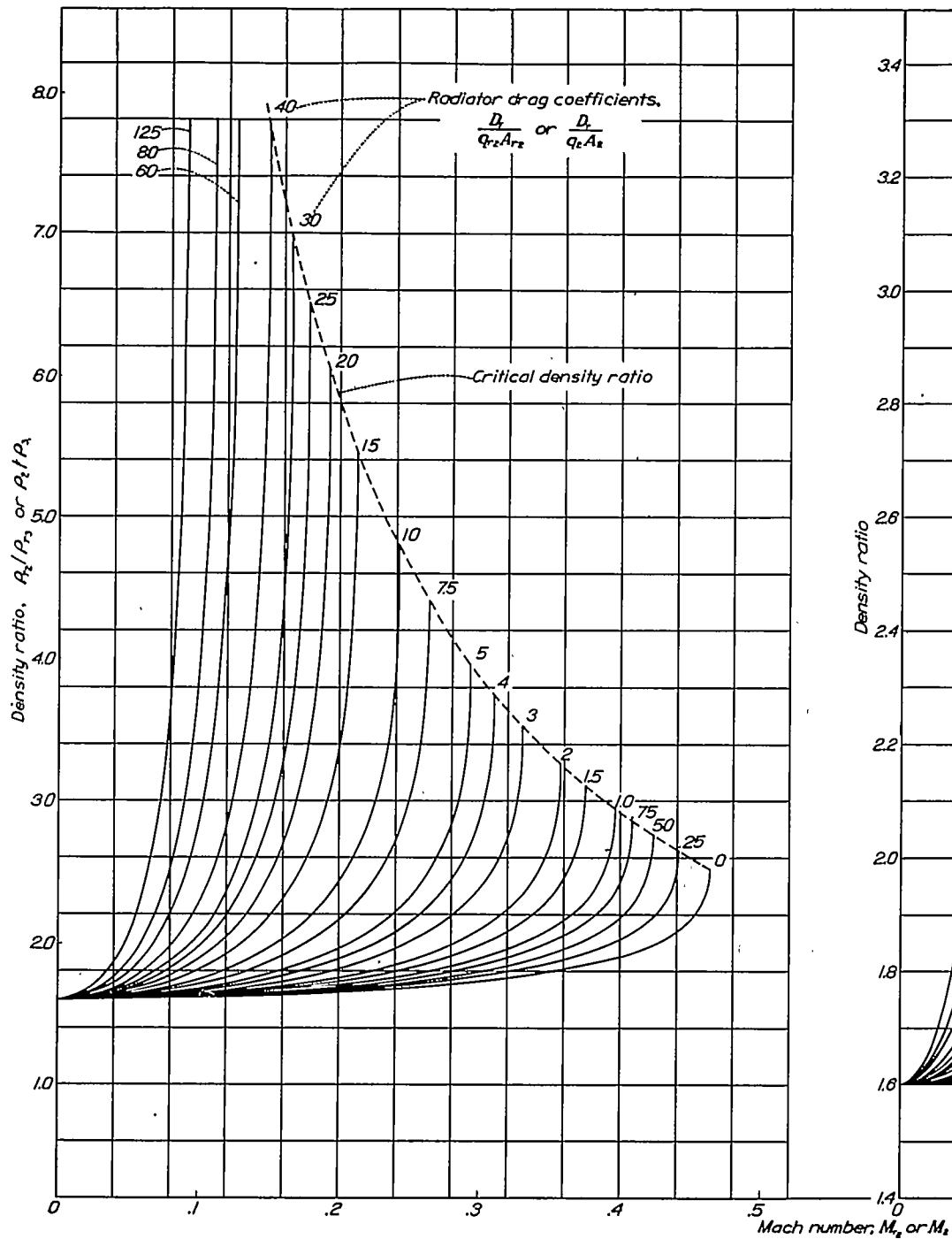
(c)  $\frac{H}{c_p g m (T_{r_2} \text{ or } T_2)} = 0.4.$

FIGURE 5.—Continued.



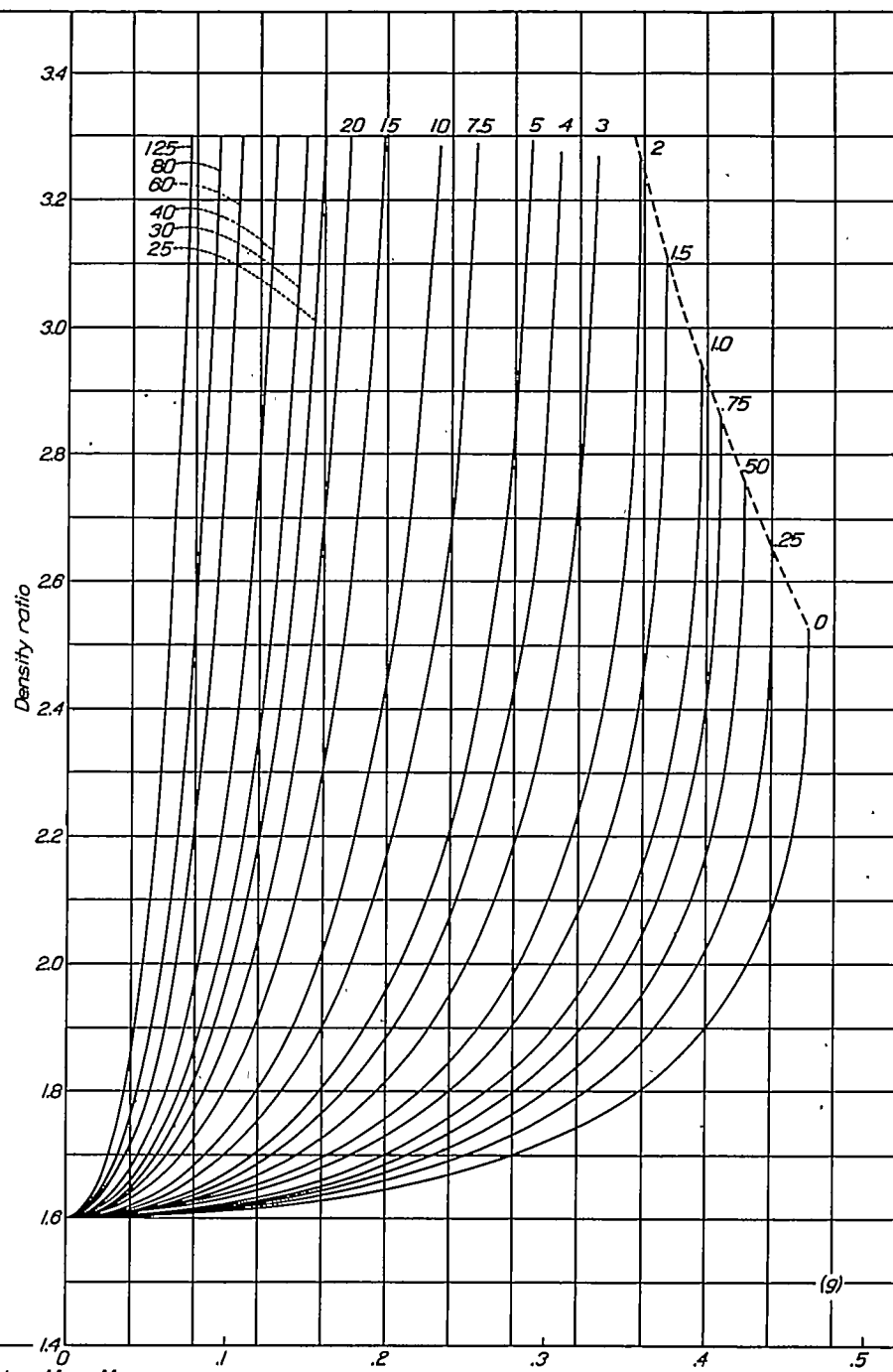
(1)  $\frac{11}{c_p \gamma m (T_1 \text{ or } T_2)} = 0.5$

FIGURE 5.—Continued.



$$(a) \frac{H}{c_p m (T_{r_2} \text{ or } T_{r_1})} = 0.0.$$

FIGURE 5.—Concluded.



(g)

With the density ratio and the drag coefficient evaluated by equations (8) and (10) as just described, the pressure drop between the entrance and exit stations of the tube is easily calculated from equation (7); that is,

$$\frac{\Delta p_t}{q_{r_2}} = C_{D_f} + 2 \left( \frac{\rho_{r_2}}{\rho_{r_3}} - 1 \right) \quad (11)$$

Flow changes across the radiator.—The pressure change between stations 2 and 3 is the sum of the pressure drop due to acceleration of the air into the tubes plus the pressure drop within the tubes less the pressure recovery between the tube exits and station 3. The pressure-recovery term has yet to be evaluated. If station 3 is assumed to be far enough behind the radiator for the velocity distribution across the duct to be uniform, the momentum equation may be applied between stations  $r_3$  and 3 to give

$$p_{r_3} - p_3 = 2q_3 \left( 1 - \frac{v_{r_3}}{v_3} \right)$$

or, as a satisfactory approximation,

$$p_{r_3} - p_3 = -2q_3 \left( \frac{A_2}{A_{r_3}} - 1 \right) \quad (12)$$

The over-all pressure drop across the radiator is the sum of equations (6), (11), and (12):

$$\Delta p_r = p_2 - p_3 = p_2 \left( 1 - \frac{p_{r_2}}{p_2} \right) + q_{r_2} \left[ C_{D_f} + 2 \left( \frac{\rho_{r_2}}{\rho_{r_3}} - 1 \right) \right] - 2q_3 \left( \frac{A_2}{A_{r_3}} - 1 \right)$$

The pressure drop is usually more conveniently expressed as a fraction of the dynamic pressure  $q_2$ , as follows:

$$\frac{\Delta p_r}{q_2} = \frac{1.43}{M_2^2} \left( 1 - \frac{p_{r_2}}{p_2} \right) + \frac{\rho_2}{\rho_{r_2}} \left( \frac{A_2}{A_{r_2}} \right)^2 \left[ C_{D_f} + 2 \left( \frac{\rho_{r_2}}{\rho_{r_3}} - 1 \right) \right] - 2 \frac{\rho_{r_2}}{\rho_{r_3}} \left( \frac{A_2}{A_{r_3}} - 1 \right) \quad (13)$$

For the case of the tubular radiator, simple methods for evaluating  $p_{r_2}/p_2$  and  $\rho_{r_2}/\rho_2$  from figures 2 and 3,  $\rho_{r_2}/\rho_{r_3}$  from figure 5, and  $C_{D_f}$  from equation (8) have been described. Equation (13) for the over-all pressure drop is exact except for the approximations made in simplifying the last term, which gives the pressure recovery between stations  $r_3$  and 3. This term is a small fraction of the over-all pressure drop and cannot be computed precisely, in most cases, because the flow distribution rarely becomes uniform in the short duct lengths that are usually available for the pressure-recovery process. With air-cooled engines, for example, the rear pressure station is always taken so close to the baffle exits that the pressure-recovery term is virtually zero and, hence, only the first two terms of equation (13) need be used. An example of the application of equation (13) to the case of a partly baffled air-cooled cylinder will be given in appendix A.

Simplified method of computing radiator pressure drop.—The pressure drop across the heated radiator can be determined by a less involved approximate method, accurate enough for many applications, which does not involve calculation of the details of the flow within the tubes or fins. The method consists of correcting the basic pressure drop

of the cold radiator to the design operating condition by a relation involving the density ratio  $\rho_2/\rho_3$  across the radiator. The use of  $\rho_2/\rho_3$  instead of the density ratio within the tubes  $\rho_{r_2}/\rho_{r_3}$  eliminates the necessity of computing the tube flow and is justified by the fact that the two ratios are approximately equal. The same general procedure followed in deriving the exact equation for the pressure drop (equation (13)) will be employed in deriving the more simple approximate relation. If  $\rho_2$  is assumed equal to  $\rho_{r_2}$ , the pressure drop between stations 2 and  $r_2$  is approximately

$$\Delta p_2 - r_2 = q_{r_2} - q_2 = q_2 \left[ \left( \frac{A_2}{A_{r_2}} \right)^2 - 1 \right]$$

Within the tube (cf. equation (7)), the pressure drop is

$$\Delta p_t = \Delta p_f + \rho_{r_3} v_{r_3}^2 - \rho_{r_2} v_{r_2}^2$$

or approximately

$$\Delta p_t = \Delta p_{f_t} \left[ \frac{1}{2} \left( 1 + \frac{\rho_2}{\rho_3} \right) \right] + 2q_2 \left( \frac{A_2}{A_{r_2}} \right)^2 \left( \frac{\rho_2}{\rho_3} - 1 \right)$$

The pressure rise between the tube exits and station 3 is (see equation (12))

$$\Delta p_{r_3-3} = -2q_2 \frac{\rho_2}{\rho_3} \left( \frac{A_2}{A_{r_2}} - 1 \right)$$

The sum of these three components is the desired over-all pressure drop; that is,

$$\begin{aligned} \Delta p_r = \Delta p_{f_t} \left[ \frac{1}{2} \left( 1 + \frac{\rho_2}{\rho_3} \right) \right] + 2q_2 \left( \frac{A_2}{A_{r_2}} \right)^2 \left( \frac{\rho_2}{\rho_3} - 1 \right) \\ + q_2 \left[ \left( \frac{A_2}{A_{r_2}} \right)^2 - 1 \right] - 2q_2 \left( \frac{\rho_2}{\rho_3} \right) \left( \frac{A_2}{A_{r_2}} - 1 \right) \end{aligned} \quad (14)$$

In order to use this relation to compute the effect of the density change across the radiator,  $\Delta p_{f_t}$  must be evaluated from the known (or calculable) value of the over-all pressure drop of the cold radiator  $\Delta p_{r_t}$ . For the basic cold condition  $\rho_2 = \rho_3$ , and equation (14) then becomes

$$\Delta p_{r_t} = \Delta p_{f_t} + q_2 \left[ \left( \frac{A_2}{A_{r_2}} \right)^2 - 1 \right] - 2q_2 \left( \frac{A_2}{A_{r_2}} - 1 \right)$$

whence

$$\Delta p_{f_t} = \Delta p_{r_t} - q_2 \left[ \left( \frac{A_2}{A_{r_2}} \right)^2 - 1 \right] + 2q_2 \left( \frac{A_2}{A_{r_2}} - 1 \right) \quad (15)$$

Thus  $\Delta p_{f_t}$  can easily be computed from the over-all pressure drop for the cold radiator if the geometry of the radiator is known. The use of equations (14) and (15) to correct the pressure drop obtained for the cold condition (or for a test condition with heat) to the design operating condition has been found to yield results approaching in accuracy the results of equation (13) in cases where the Mach number of the flow in the tubes is not large. As previously discussed, the last term in both equations (14) and (15) should not be included in cases where station 3 is too close to the tube exits to permit the velocity distribution to become uniform.

In order to obtain the correct value of  $\rho_2/\rho_3$  for use in equation (14), it is important that compressibility effects, as well as heating effects, be allowed for. A simple method of obtaining  $\rho_2/\rho_3$  from figure 5 will now be presented. For this method the drag coefficient of the radiator  $C_{D_r}$  will be needed, and this value can be obtained from equation (14) as follows (cf. equation (11)):

$$C_{D_r} = \frac{D_r}{q_2 A_2} = \frac{\Delta p_r}{q_2} - 2 \left( \frac{\rho_2}{\rho_3} - 1 \right) \quad (16)$$

where  $\Delta p_r/q_2$  is given by equation (14). The flow in the constant-area duct between stations 2 and 3 is analogous to the flow in the tubes and exactly the same relations apply between stations 2 and 3 as have been applied between stations  $r_2$  and  $r_3$ . Equations (7), (9), (10), and (11) may thus be used to compute the density ratio  $\rho_2/\rho_3$  and the pressure drop across the radiator by merely changing the notation to represent the duct flow rather than the tube flow. Similarly, figure 5, which is a graphical representation of equation (10), may be used to obtain  $\rho_2/\rho_3$  directly. The aforementioned changes in notation, applicable to equations (7) to (11) and to figure 5, are as follows:

Replace  $M_{r_2}$  by  $M_2$

Replace  $\rho_{r_2}/\rho_{r_3}$  by  $\rho_2/\rho_3$

Replace  $\frac{H}{c_p g m T_{r_2}}$  by  $\frac{H}{c_p g m T_2}$

Replace  $\frac{D_{friction}}{q_{r_2} A_{r_2}}$  by  $\frac{D_{radiator}}{q_2 A_2}$ , or  $C_{D_r}$  by  $C_{D_r}$

Figure 5 may be used with the revised notation to obtain a value for  $\rho_2/\rho_3$ . By use of a trial value of  $\rho_2/\rho_3$ , the drag coefficient  $C_{D_r}$  can be determined from equation (16). With this value of  $C_{D_r}$ , a new value of  $\rho_2/\rho_3$  can be determined from figure 5. This process is repeated until corresponding values of  $C_{D_r}$  and  $\rho_2/\rho_3$  are obtained. Equation (14) may be then evaluated for the radiator pressure drop.

For design work, it is frequently necessary to compute the pressure-drop ratio  $\Delta p_r/q_0$ . This quantity can be written in the form

$$\frac{\Delta p_r}{q_0} = \frac{\Delta p_r}{q_2} \left( \frac{q_2}{q_0} \right)$$

which can be evaluated in terms of the flight Mach number and the design area ratio  $A_0/A_2$  in cases where the area ratio is small (say less than 0.2) and where the diffuser loss may be neglected. For these conditions, from equation (3) or figure 3,

$$\frac{\rho_0}{\rho_2} = \left( \frac{1}{1 + 0.20 M_0^2} \right)^{2.5}$$

Therefore,

$$\frac{q_2}{q_0} = \frac{\rho_2}{\rho_0} \left( \frac{\rho_0 A_0}{\rho_2 A_2} \right)^2 = \left( \frac{1}{1 + 0.20 M_0^2} \right)^{2.5} \left( \frac{A_0}{A_2} \right)^2$$

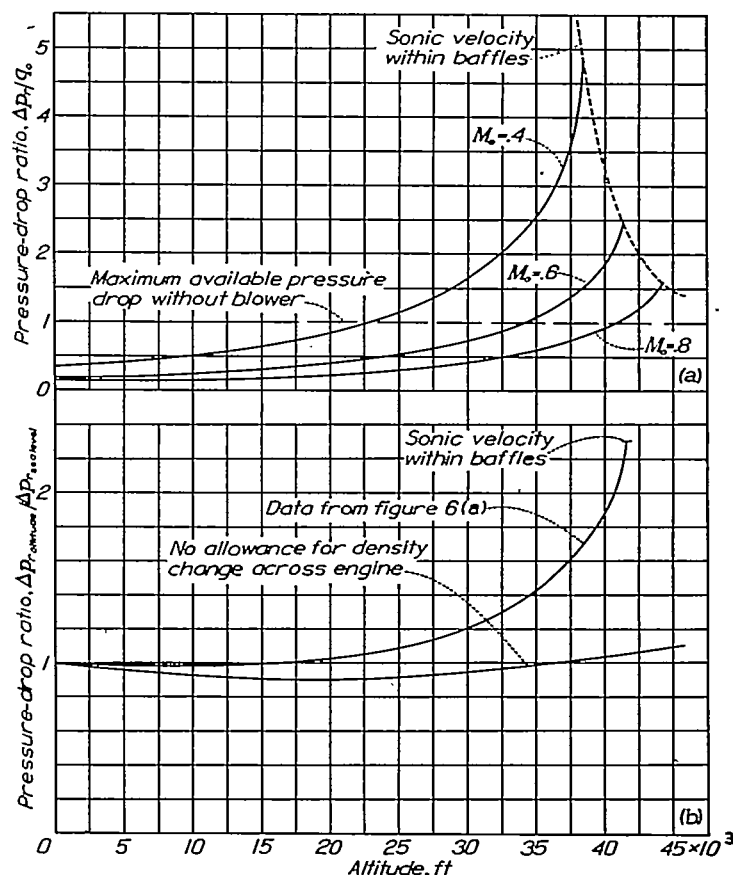
and

$$\frac{\Delta p_r}{q_0} = \left( \frac{1}{1 + 0.20 M_0^2} \right)^{2.5} \left( \frac{A_0}{A_2} \right)^2 \frac{\Delta p_r}{q_2} \quad (17)$$

Either the approximate value of  $\Delta p_r/q_2$  given by equation (14) or the exact value from equation (13) may be used in equation (17). The quantities  $A_0/A_2$  and  $M_0$  are design constants.

It has been shown in figure 5 that the density ratio across a radiator or air-cooled engine becomes very large as the tube or duct Mach numbers increase, even with low rates of heating. Corresponding increases in friction and in the pressure drop due to momentum increase within the tubes have been indicated in equation (13) or (14). These adverse effects due to the density-ratio change should be emphasized because, under present-day operating conditions at high altitude, very large Mach numbers can be obtained within radiators and, in particular, within the baffles of air-cooled engines. Calculation of the required pressure drops will be seriously in error if no allowance is made for the effects of density change. Equation (13) or (14) or equivalent relations must be used. High-speed test data are needed to indicate how closely the one-dimensional analysis of this report approximates the actual flow through an air-cooled engine.

In order to illustrate the large pressure-drop increase that will be required as the operating altitude is increased, figure 6 has been prepared for a typical existing air-cooled engine. Figure 6(a) shows the variation of the pressure-drop ratio  $\Delta p_r/q_0$  with altitude for the air-cooled engine.



(a) Pressure-drop ratio in terms of dynamic pressure  $\Delta p_r/q_0$ .

(b) Pressure-drop ratio in terms of sea-level conditions.  $M_0=0.6$

FIGURE 6.—Variation of pressure-drop ratio with altitude for a typical air-cooled engine. Engine conditions assumed are full-rated power; fuel-air ratio, 0.10; maximum head temperature, 450° F.

Two limiting conditions beyond which the desired cooling conditions cannot be maintained are included. The first occurs when the maximum available pressure drop (assumed as  $1.0q_0$  with extended exit flaps) is reached. Flight at an altitude higher than the altitude defined by this limit would require the use of a blower. If a blower were used, the second limiting condition would occur at a still higher altitude, where sonic velocity would be attained within the baffles. A comparison is made in figure 6(b) of the increase in pressure drop with altitude as predicted by the methods of this report with the increase predicted by current methods in which no allowance is made for the density change across the engine. Details of the calculation and the assumptions involved are given in appendix A.

A study of the effects of increasing the fin area of the engine indicates that the cooling difficulties shown on figure 6(a) could be delayed to altitudes higher than those indicated if the fin area could be increased. The same result could be obtained by the unsatisfactory expedient of increasing either the fuel-air ratio or the head temperature. This fact undoubtedly explains the ability of some existing airplanes to operate at very high altitudes for limited periods of time. It is also evident that the cooling problem is alleviated by the reduction in power output that occurs if the critical altitude of supercharging is exceeded.

Temperature change across radiator.—The temperature rise across the heating device is easily calculated after the pressure drop and density ratio  $\rho_2/\rho_3$  have been obtained. The desired temperature-rise ratio  $\Delta t_r/T_2$  is derived as follows:

$$\begin{aligned} \frac{T_3}{T_2} &= \frac{\rho_3}{\rho_2} \frac{\rho_2}{\rho_3} \\ \frac{T_3 - T_2}{T_2} &= \frac{\Delta t_r}{T_2} = \frac{\rho_3}{\rho_2} \frac{\rho_2}{\rho_3} - 1 \\ \frac{\Delta t_r}{T_2} &= \left(1 - \frac{\Delta p_r}{q_2} \frac{q_2}{\rho_3}\right) \frac{\rho_2}{\rho_3} - 1 \end{aligned} \quad (18)$$

where  $\Delta p_r/q_2$  is given by equation (13) or (14) and  $\rho_2/\rho_3$  is obtained from the chart (fig. 5) using the duct-flow notation.

Station 3.—If either equation (13) or (14) is used to compute the pressure drop and equation (18) is used to compute the temperature change, the conditions at station 3 are given by

$$\begin{aligned} p_3 &= p_2 - \left(\frac{\Delta p_r}{q_0}\right) q_0 \\ T_3 &= T_2 + \left(\frac{\Delta t_r}{T_2}\right) T_2 \\ \rho_3 &= 0.000583 \frac{p_3}{T_3} \\ M_3 &= M_0 \frac{\rho_0}{\rho_3} \frac{A_0}{A_3} \left(\frac{T_0}{T_3}\right)^{1/2} \end{aligned}$$

Station 4.—The internal static pressure at station 4 depends on the shape and location of the outlet. Efficient

outlets of the type employed in the present tests are designed to make the streamlines of both the internal and external flows as nearly parallel as possible at the outlet; thus, the external outlet pressure becomes equal to the internal pressure. (See references 4 and 7.) The value of the outlet pressure for this type of outlet is found to be about the same as the pressure existing at that station on the body before the opening was added. Pressure-distribution data for faired bodies may therefore be used to estimate the outlet pressure for openings of the type described. If the walls of the outlet are converging rather than parallel, however, the outlet pressure will be considerably higher than the pressure on the corresponding faired body. (See references 4 and 7.) With cusped outlets at the tail of the streamline body, as assumed for the present analysis, the outlet pressure is about  $0.11q_0$  above stream static pressure, according to reference 5. If an estimate of the outlet pressure is made as suggested, the flow conditions at the outlet may be computed from

$$\begin{aligned} p_4 &= p_0 + P_4 q_0 \\ T_4 &= T_3 \left(\frac{p_4}{p_3}\right)^{\frac{\gamma-1}{\gamma}} = T_3 \left(\frac{p_4}{p_3}\right)^{0.286} \\ \rho_4 &= 0.000583 \frac{p_4}{T_4} \end{aligned}$$

or

$$\rho_4 = \rho_3 \left(\frac{p_4}{p_3}\right)^{1/\gamma}$$

The size of the opening required to permit passage of the design quantity of internal flow can now be computed from

$$A_4 = \frac{m}{\rho_4 v_4} \quad (19)$$

where  $m$  is known,  $\rho_4$  has been given previously, and  $v_4$  is given by

$$\begin{aligned} v_4 &= \sqrt{v_3^2 + \frac{2\gamma}{\gamma-1} \frac{p_3}{\rho_3} \left[1 - \left(\frac{p_4}{p_3}\right)^{\frac{\gamma-1}{\gamma}}\right]} \\ &= \sqrt{\left(\frac{m}{\rho_3 A_3}\right)^2 + 7.0 \frac{p_3}{\rho_3} \left[1 - \left(\frac{p_4}{p_3}\right)^{0.286}\right]} \end{aligned} \quad (20)$$

The assumption of isentropic flow between stations 3 and 4 yields accurate results for unobstructed outlet passages. In ordinary cases the effects of friction are localized in a shallow boundary layer near the wall and do not affect the main outlet flow. In many practical arrangements, however, the outlet passage is complicated by turns, tiers of guide vanes, and like arrangements, to which special consideration must be given. In such cases, it is suggested that the step-by-step process employed in determining the flow across the radiator be used. The drag coefficient of the obstruction can usually be estimated and figure 5 may be used to simplify the computations.

A less exact but more simple method of accounting for the energy loss due to obstructions between stations 3 and 4 assumes that the isentropic expansion takes place between

the pressure  $p_3 - \Delta h_{3-4}$  and the outlet pressure, where  $\Delta h_{3-4}$  is the total-pressure loss occurring between stations 3 and 4; that is, as an approximation,

$$\rho_4 = \rho_3 \left( \frac{p_4}{p_3 - \Delta h_{3-4}} \right)^{1/\gamma}$$

A sample calculation using this method was given in reference 8.

For usual installations, the maximum duct velocity between stations 3 and 4 will be attained at the outlet. It can be shown that the outlet Mach number cannot exceed unity. This limiting condition cannot be reached in ordinary cases, however, without the aid of an internal blower because the outlet Mach number will not exceed the flight Mach number except in systems where the outlet is located in a region of high negative pressure. The addition of heat alone will not appreciably change the outlet Mach number because, with the increase in outlet velocity due to the addition of heat, there is a corresponding increase in the speed of sound. If the critical velocity were reached in the outlet, the mass-flow rate could still be increased by an increase in outlet area.

Station 5.—The velocity at station 5 is required for the purpose of computing the resultant force due to the internal flow. As the static pressure is equal to  $p_0$ , by the general energy equation

$$v_5 = \sqrt{\left( \frac{m}{\rho_4 A_4} \right)^2 + 7.0 \left( \frac{p_4}{\rho_4} \right) \left[ 1 - \left( \frac{p_0}{p_4} \right)^{0.286} \right]}$$

The resultant force is obtained by substitution of this value of  $v_5$  into the momentum relation which, since  $p_5 = p_0$ , is simply

$$D = m(V_0 - v_5) \quad (21)$$

A negative result obviously indicates that the resultant force is a thrust.

#### THE EFFECTS OF HEAT AND COMPRESSIBILITY ON THE TOTAL PRESSURE AT THE OUTLET AND ON THE INTERNAL MASS FLOW

Total pressure at the outlet.—In cases where the station-to-station method is not employed, the total pressure at the outlet must be measured or calculated in order to determine the net drag or thrust due to the internal flow. The station-to-station method of analysis just described, although essential in calculating exactly the details of the internal flow, does not clearly indicate the over-all effects of heating and compressibility on the outlet total pressure. A more direct method, which is useful in illustrating the effects in question and also in computing the mass-flow changes and the net thrust, will now be described. The total-pressure loss at the outlet is the sum of the loss across the radiator, the duct loss, and the pressure rise through the blower, if one is present; that is,

$$\left( \frac{\Delta h}{q_0} \right)_{\text{over-all}} = \left( \frac{\Delta h}{q_0} \right)_r + \left( \frac{\Delta h}{q_0} \right)_{\text{duct}} + \left( \frac{\Delta h}{q_0} \right)_{\text{blower}} \quad (22)$$

The total-pressure loss across the radiator is equal to the static-pressure drop (equation (17)) less the dynamic-pressure rise (for the small values of  $M_2$  usually encountered).

$$\left( \frac{\Delta h}{q_0} \right)_r = \left( \frac{\Delta p}{q_0} \right)_r - \frac{q_3 - q_2}{q_0} = \left( \frac{\Delta p}{q_0} \right)_r - \frac{q_2}{q_0} \left( \frac{\rho_2}{\rho_3} - 1 \right)$$

From equation (17), therefore, if no blower is used,

$$\left( \frac{\Delta h}{q_0} \right)_{\text{over-all}} = \left( \frac{A_0}{A_2} \right)^2 \left( \frac{1}{1 + 0.20 M_0^2} \right)^{2.5} \left[ \frac{\Delta p_r}{q_2} - \left( \frac{\rho_2}{\rho_3} - 1 \right) \right] + \left( \frac{\Delta h}{q_0} \right)_{\text{duct}} \quad (23)$$

This equation is easily evaluated by use of figure 5 with the duct-flow notation to obtain the necessary values of  $\rho_2/\rho_3$ . The duct loss should include an estimate of the skin-friction losses plus the diffuser loss, which, from equation (5), is given by

$$\left( \frac{\Delta h}{q_0} \right)_{\text{diffuser}} = \frac{q_1}{q_0} \left[ 1 - \left( \frac{A_1}{A_d} \right)^2 \right] (1 - \eta_d)$$

For a constant mass-flow ratio  $A_0/A_2$ , the radiator drag increases as a result of the increase in density ratio  $\rho_2/\rho_3$  due to heating. As shown by equation (23), the total-pressure loss will correspondingly increase. Aside from this well-known effect, however, the addition of heat will cause little change in the outlet total pressure. From the development leading to equation (23), it is seen that, for a given mass flow and radiator drag, the outlet total pressure will decrease as heat is added by the amount  $q_3 - q_2$ . Owing to the low duct velocities, the quantity  $(q_3 - q_2)/q_0$  will be very small in usual cases. This result is of considerable interest in that measurement of total pressure in the wake will give no direct indication of the propulsive effect of heating.

When the duct velocities are large, however, and the corresponding value of  $q_3 - q_2$  is appreciable, the foregoing development indicates that the effect of heat will cause an appreciable loss in outlet total pressure over and above the increased radiator drag loss.

For a duct system with moderate internal losses, no appreciable drag change of surfaces exposed to the outlet flow is to be expected because of the negligibly small change in outlet dynamic pressure with heating. The Reynolds number of the outlet flow decreases, however, and some scale effect might therefore be expected. No change in the outlet Mach number occurs because the velocity increase is offset by an increase of the speed of sound in the heated outlet flow.

Variation of mass flow.—The internal mass-flow coefficient  $\frac{m}{\rho_0 F V_0}$  or the flow ratio  $\frac{\rho_4 v_4}{\rho_0 V_0}$  is a constant for a given system, except for the effects of compressibility and heating. (See reference 5.) In order to show these effects, the ratio  $\frac{\rho_4 v_4}{\rho_0 V_0}$  will be written in terms of  $M_0$  and  $\frac{H}{c_p g_m T_0}$ . From the

general energy equation,

$$\frac{\rho_4 v_4^2}{2} = \frac{\gamma}{\gamma-1} P_4 \left[ \left( \frac{h_4}{p_4} \right)^{\frac{\gamma-1}{\gamma}} - 1 \right]$$

whence,

$$\frac{\rho_4 v_4}{\rho_0 V_0} = \sqrt{\frac{\gamma}{\gamma-1} \frac{p_4}{\rho_0} \frac{p_4}{q_0} \left[ \left( \frac{h_4}{p_4} \right)^{\frac{\gamma-1}{\gamma}} - 1 \right]} \quad (24)$$

where

$$\frac{h_4}{p_4} = \frac{h_0 - \Delta h}{p_4} = \frac{p_0}{p_4} \left( 1 + \frac{\gamma-1}{2} M_0^2 \right)^{\frac{\gamma}{\gamma-1}} - \frac{\Delta h}{p_4}$$

and

$$p_4 = p_0 + P_4 q_0 = p_0 \left( 1 + \frac{\gamma M_0^2}{2} P_4 \right)$$

The density ratio  $\rho_4/\rho_0$  in equation (24) can be written in terms of the heat added and  $M_0$ .

When the indicated substitutions for total pressure are made, equation (24) becomes

$$\frac{\rho_4 v_4}{\rho_0 V_0} = \sqrt{\frac{p_4}{\rho_0}} \sqrt{\frac{\gamma}{\gamma-1} \left( \frac{2 + \gamma P_4 M_0^2}{\gamma M_0^2} \right) \left\{ \left[ \left( \frac{2}{2 + \gamma P_4 M_0^2} \right) \left( 1 + \frac{\gamma-1}{2} M_0^2 \right)^{\frac{\gamma}{\gamma-1}} - \left( \frac{\Delta h/q_0}{\gamma M_0^2} \right)^{\frac{\gamma-1}{\gamma}} \right] - 1 \right\}} \quad (26)$$

where  $\rho_4/\rho_0$  is given by equation (25). Inspection of this result shows that, for fixed values of  $M_0$  and  $\Delta h/q_0$ , the mass flow will decrease as heat is applied in proportion to  $\rho_4^{1/2}$ . The outlet area, therefore, must be increased as heat is added to the flow if a fixed mass-flow rate is to be maintained. Equation (26) has been solved for a range of values of  $\Delta h/q_0$  and  $M_0$  in order to show the effect of Mach number and to facilitate the use of this relation in design work. The solution is shown on figure 7 for an outlet pressure equal to free-stream static pressure  $P_4=0$ . The Mach number effect on the flow ratio is seen to be appreciable. Equation (26) or figure 7 will yield values of  $\rho_4 v_4$  as accurate as the results of the step-by-step process for most applications, provided that the internal losses are not excessive and that the heat is added at a duct pressure approaching stagnation pressure. The values of  $\Delta h/q_0$  and  $\rho_4/\rho_0$  required for solution of equation (26) or for use with figure 7 are obtained from equations (23) and (25), respectively.

If the flow is considered to be incompressible except for the effect of heating, equation (26) can be reduced to

$$\frac{\rho_4 v_4}{\rho_0 V_0} = \left( \frac{p_4}{\rho_0} \right)^{1/2} \left( 1 - \frac{\Delta h}{q_0} - P_4 \right)^{1/2} \quad (27)$$

as  $M_0$  approaches zero. This relation was given in reference 7. The curve on figure 7 for  $M_0=0$  is a plot of equation (27) for the outlet pressure coefficient  $P_4=0$ . Because of its simplicity and also because equation (26) tends to become inaccurate at very low Mach numbers, equation (27) should be used for  $M_0 < 0.2$  in preference to equation (26) in cases where figure 7 is not used. Figure 7 applies for only one value of the outlet pressure coefficient  $P_4=0$ . It may be used for values of  $P_4$  other than 0, by correcting the result obtained from the figure to the required value of  $P_4$  according to equation (27).

Direct calculation of the outlet area.—Calculation of the size of outlet opening required to pass the design mass flow is one of the most frequently performed operations in the

$$\frac{\rho_4}{\rho_0} = \frac{\rho_5}{\rho_0} \frac{\rho_4}{\rho_5} = \frac{T_0}{T_5} \left( \frac{p_4}{p_0} \right)^{1/\gamma} = \frac{T_0}{T_5} \left( 1 + \frac{\gamma P_4 M_0^2}{2} \right)^{1/\gamma}$$

If the internal losses are assumed to be moderate and the pressure at the radiator to approach stagnation pressure, it can be shown from the energy relations that  $T_5$  is related to the heat added as follows:

$$\frac{T_0}{T_5} = \frac{1}{1 + \frac{H}{c_p g m T_0 (1 + 0.20 M_0^2)}}$$

whence

$$\frac{\rho_4}{\rho_0} = \frac{(1 + 0.7 P_4 M_0^2)^{0.714}}{1 + \frac{H}{7.74 m T_0 (1 + 0.20 M_0^2)}} \quad (25)$$

design of an internal flow system. If the step-by-step process has been carried out, the outlet area may be calculated from the values of  $\rho_4$  and  $v_4$  as already shown (equation (19)). In general, however, the computation of  $A_4$  without the detailed intermediate steps is desirable. Equation (25), with equation (26) or (27), or figure 7 can be used to calculate  $\frac{\rho_4 v_4}{\rho_0 V_0}$ , which permits the outlet area to be obtained directly:

$$A_4 = \frac{m}{\rho_4 v_4} = \frac{m}{\left( \frac{\rho_4 v_4}{\rho_0 V_0} \right) \rho_0 V_0}$$

or

$$A_4 = \frac{A_0}{\left( \frac{\rho_4 v_4}{\rho_0 V_0} \right)} \quad (28)$$

Effect of an operating propeller.—If the inlet opening is located in the slipstream, the velocity, the pressure, and the density in the slipstream should be taken as the initial conditions and the same procedure followed as for the condition without propeller in arriving at the conditions in the duct. In cases where the inlet is immediately behind the propeller, it will be found convenient to take the flow characteristics in the inlet opening as the initial conditions rather than the conditions ahead of the propeller. The area-ratio charts (figs. 2, 3, and 4) may be used after substitution of  $A_1$  and  $M_1$  for  $A_0$  and  $M_0$ .

THE CONVERSION OF HEAT ENERGY TO THRUST POWER

The effects of the addition of heat in increasing the radiator drag and in reducing the internal mass flow have been discussed. Both of these effects cause changes in the drag due to the internal losses, but neither effect results from the recovery of mechanical energy from the heat added. In the study of the propulsive effect due to heating, therefore, it is desirable to eliminate these unrelated drag changes. This elimination can be accomplished by assuming, for comparison with the heated condition, a hypothetical condition without heat in which both the radiator drag and the

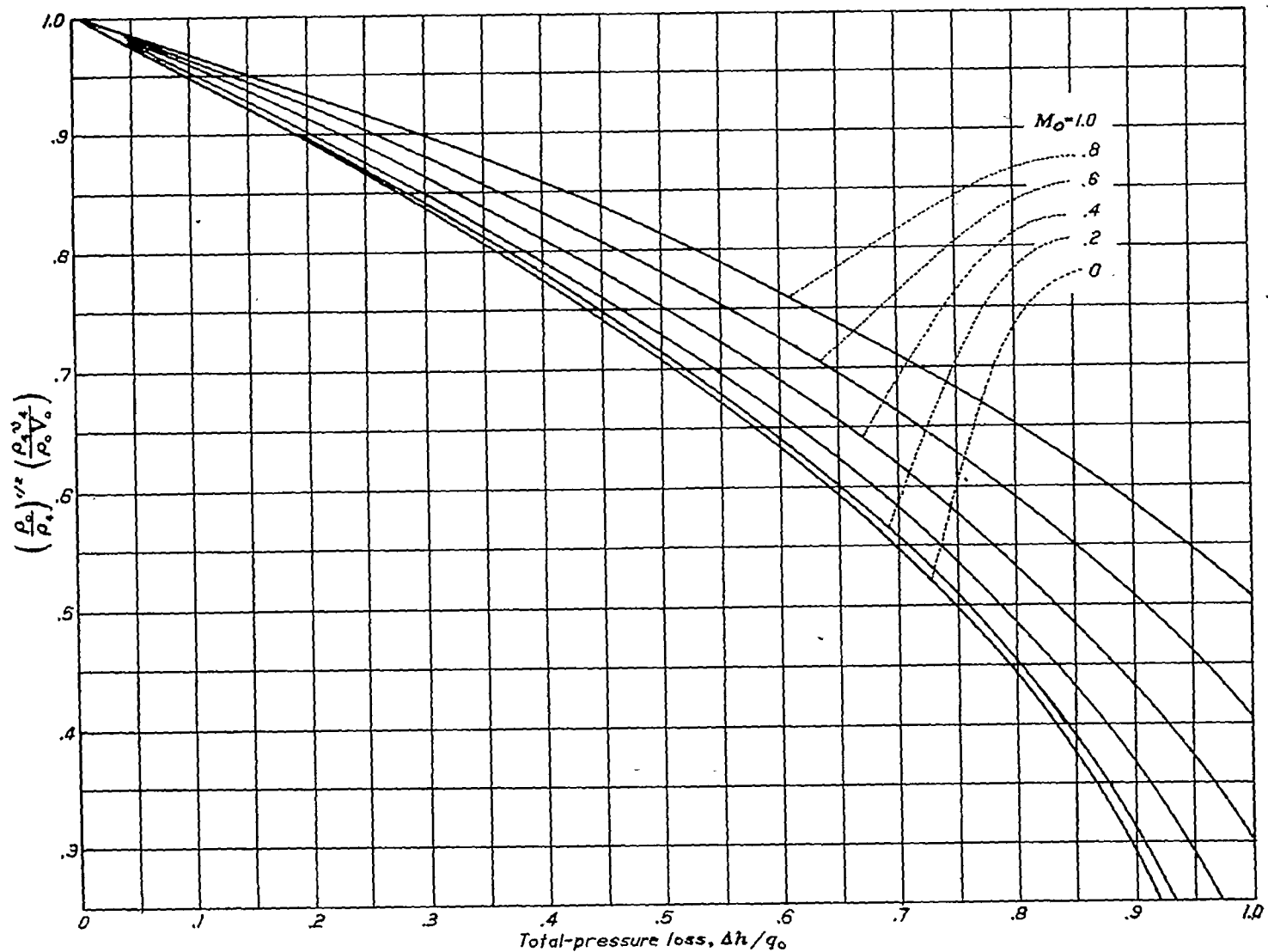


FIGURE 7.—Curves for determining the outlet velocity ratio.  
(Solution of equation (26) for  $P_1=0$ .)

mass-flow rate have the same values as in the heated condition. This assumption not only simplifies the analysis of the recovery process but also greatly facilitates calculation of the net propulsive force, as will presently be shown. In the following analysis this assumed unheated condition will be indicated by the use of primes with the symbols.

The net drag due to the flow through an internal system is equal to the decrease in the momentum of the internal flow, provided that the momentum is measured at stations where the static pressures are equal to free-stream pressure.

From equation (21),

$$D = m(V_0 - v_s)$$

If the system produces a net thrust, this thrust is given by the increase in momentum of the internal flow:

$$T = -D = m(v_s - V_0)$$

The drag, decrease (or thrust increase) resulting from the recovery of mechanical energy from the addition of heat is

$$\Delta T = (\text{Thrust with heat}) - (\text{Thrust without heat but with same mass flow and same radiator drag as with heat})$$

or

$$\Delta T = m(v_s - v_s') \quad (29)$$

The increase in kinetic energy of the internal flow due to the recovery process is thus

$$\Delta(K. E.) = \frac{m}{2}(v_s^2 - v_s'^2) \quad (30)$$

If the efficiency of the process is defined as

$$\epsilon_H = \frac{K. E. \text{ recovered}}{\text{Total heat added}}$$

Then, from equation (30),

$$\epsilon_H = \frac{m(v_s^2 - v_s'^2)}{2JH} \quad (31)$$

The over-all efficiency of conversion of heat energy into thrust power is the ratio

$$\epsilon_T = \frac{\text{Useful thrust power}}{\text{Heat added}} = \frac{\Delta T V_0}{JH} = \frac{m(v_s - v_s') V_0}{JH} \quad (32)$$

This equation can be written in terms of the heat-cycle efficiency (equation (31)) as follows:

$$\epsilon_T = \epsilon_H \left( \frac{2V_0}{v_5 + v_5'} \right) = \epsilon_H \epsilon_M \quad (33)$$

The quantity  $\epsilon_M$  represents the efficiency with which the kinetic energy recovered from the heat input is converted into thrust power. This efficiency is analogous to the ideal efficiency of a propeller and, in the same way, accounts for the energy left in the wake when the wake velocity is different from  $V_0$ . It will be found convenient in the succeeding analysis to express  $\epsilon_M$  in terms of the internal-drag coefficients with and without heat. From equations (21) and (33), expressing the drag and mass flow in coefficient form,

$$\epsilon_M = \frac{1}{1 - \frac{1}{4C} (C_D + C_D')} \quad (34)$$

**Efficiency of the heat-recovery cycle.**—If the duct velocity at the radiator section is very small in comparison with the flight velocity, the static pressure at which heat is added will approach stagnation pressure and the pressure change across the radiator will approach zero. Under these conditions the heat cycle consists of an adiabatic compression from the stream static pressure to stagnation pressure, an addition of heat at constant pressure ( $p_2 \approx p_r \approx p_3$ ), and an adiabatic expansion back to  $p_0$ . The continual admission of air at pressure  $p_0$  and density  $\rho_0$  is equivalent to cooling the outlet flow back to  $\rho_0$  at constant pressure  $p_0$  and this step completes the cycle. This process corresponds to an ideal heat engine cycle, the efficiency of which is, from elementary thermodynamic relations,

$$\epsilon_H = \frac{\text{Kinetic energy recovered}}{\text{Total heat added}} = 1 - \left( \frac{p_2}{p_0} \right)^{\frac{1-\gamma}{\gamma}} \quad (35)$$

The assumptions on which this formula is based are justified in the case of the internal flow system only when the duct velocities are very small by comparison with the flight speed and when the friction losses in the radiator or combustion chamber are negligible. Operating conditions exist, however, in which relatively high duct velocities occur, and an expression for the efficiency applicable to such cases will now be derived. The heat-cycle efficiency will be shown to depend not only on the compression ratio but also on the Mach number of the duct flow and on the rate of heating.

From the energy equation (cf. equation (9)),

$$\frac{v_5^2 - v_5'^2}{2} = \frac{JH}{m} - Jg_c p (T_5 - T_5')$$

By equation (31), therefore,

$$\epsilon_H = 1 - \frac{c_p g_m}{H} (T_5 - T_5') \quad (36)$$

The values of  $T_5$  and  $T_5'$  will depend on the outlet pressure and on the conditions at station 3, which in the general case will depend on  $M_2$  and on the radiator or combustion-chamber

losses. The previous analysis has indicated that when a radiator of conventional design is present it is impossible to obtain high Mach numbers in the duct at station 2 because the flow will choke within the radiator at the tube exits for relatively low values of  $M_2$ . Since it is desired in the present analysis to show the effects of relatively large increases in  $M_2$  on the efficiency of the recovery cycle, it will be assumed that no radiator obstructs the duct. The addition of heat will be assumed to take place by combustion of fuel in the duct between stations 2 and 3 by means of a burner having negligible friction losses. This ideal arrangement is being approached in the ram-jet types of propulsion system. The effects of the increase in mass flow due to addition of fuel are of secondary importance and will be neglected. From these assumptions  $T_5'$  can be related to  $T_2$  as follows:

$$T_5' = T_2 \left( \frac{p_2}{p_0} \right)^{\frac{1-\gamma}{\gamma}}$$

The pressure  $p_3$  is less than  $p_2$  by the value of the momentum increase due to the addition of heat; that is, inasmuch as  $A_2 = A_3$

$$p_3 = p_2 - \rho_2 v_2^2 \left( \frac{\rho_2}{\rho_3} - 1 \right)$$

$$\frac{p_3}{p_2} = 1 - \gamma M_2^2 \left( \frac{\rho_2}{\rho_3} - 1 \right)$$

Also, from the equation of state,

$$T_3 = T_2 \frac{p_2}{p_3} \frac{\rho_3}{\rho_2}$$

and, substituting for  $p_3/p_2$ ,

$$T_3 = T_2 \frac{p_2}{p_3} \left[ 1 - \gamma M_2^2 \left( \frac{\rho_2}{\rho_3} - 1 \right) \right]$$

Now,

$$T_5 = T_3 \left( \frac{p_3}{p_0} \right)^{\frac{1-\gamma}{\gamma}}$$

$$\begin{aligned} T_5 &= T_2 \frac{p_2}{p_3} \left[ 1 - \gamma M_2^2 \left( \frac{\rho_2}{\rho_3} - 1 \right) \right] \left( \frac{p_3}{p_0} \right)^{\frac{1-\gamma}{\gamma}} \left[ 1 - \gamma M_2^2 \left( \frac{\rho_2}{\rho_3} - 1 \right) \right]^{\frac{1-\gamma}{\gamma}} \\ &= T_2 \frac{p_2}{p_3} \left( \frac{p_2}{p_0} \right)^{\frac{1-\gamma}{\gamma}} \left[ 1 - \gamma M_2^2 \left( \frac{\rho_2}{\rho_3} - 1 \right) \right]^{1/\gamma} \end{aligned}$$

The heat-cycle efficiency is, therefore, from equation (36)

$$\epsilon_H = 1 - \left( \frac{1}{H} \right) \left( \frac{p_2}{p_0} \right)^{\frac{1-\gamma}{\gamma}} \left\{ \frac{p_2}{p_3} \left[ 1 - \gamma M_2^2 \left( \frac{\rho_2}{\rho_3} - 1 \right) \right]^{1/\gamma} - 1 \right\} \quad (37)$$

This equation for  $\epsilon_H$  is plotted in figure 8 as a function of compression ratio for various values of the heat input factor and  $M_2$ . The term  $\rho_2/\rho_3$  in equation (37) is a function only of these variables and was computed from equation (10) for  $C_{D_r} = 0$ , using notation appropriate to the duct rather than the radiator tube.

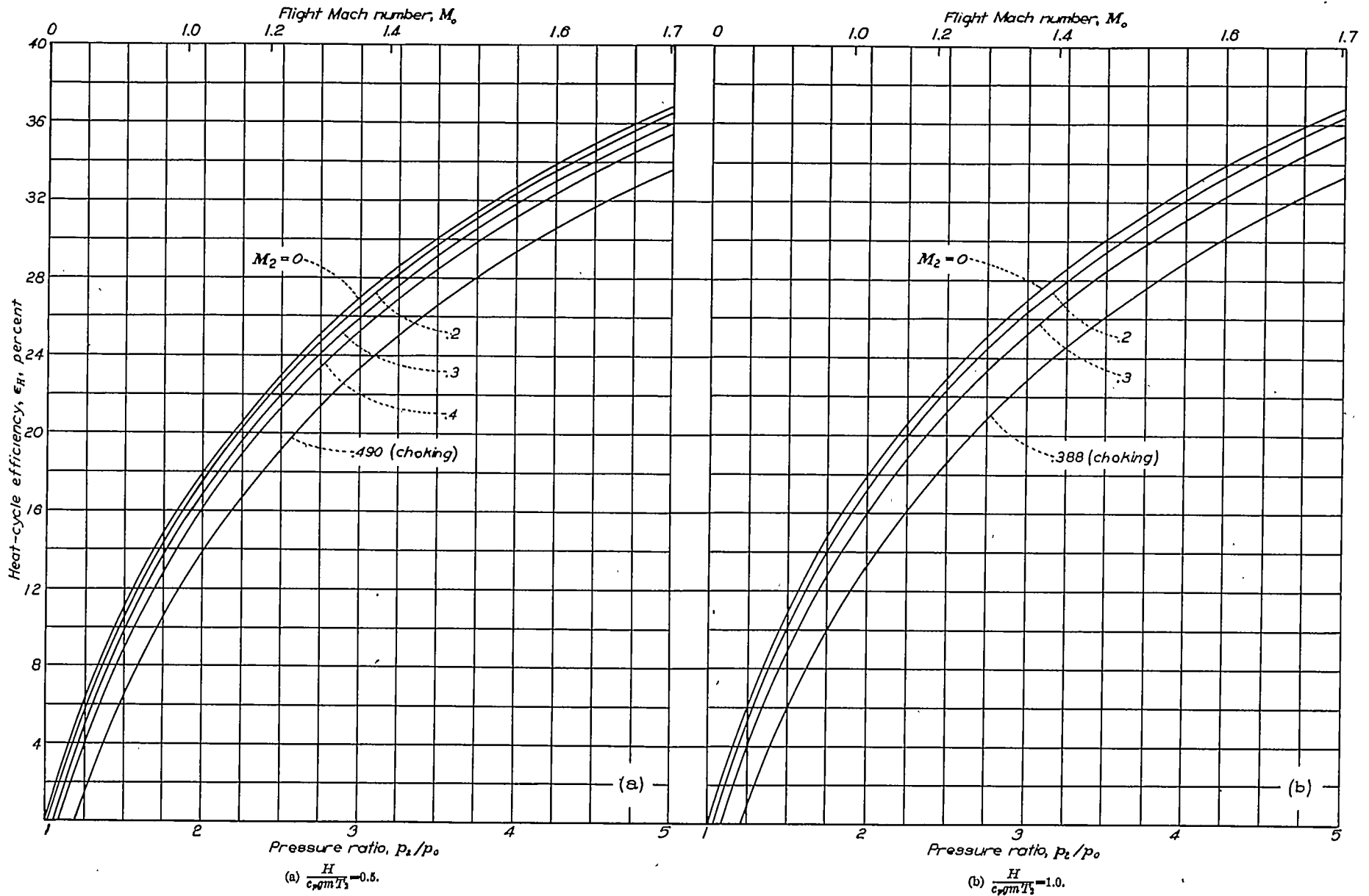


FIGURE 8.—Variation of heat-cycle efficiency with pressure ratio and flight Mach number for various internal Mach numbers at station 2.  $C_{D_p} = 0$ .

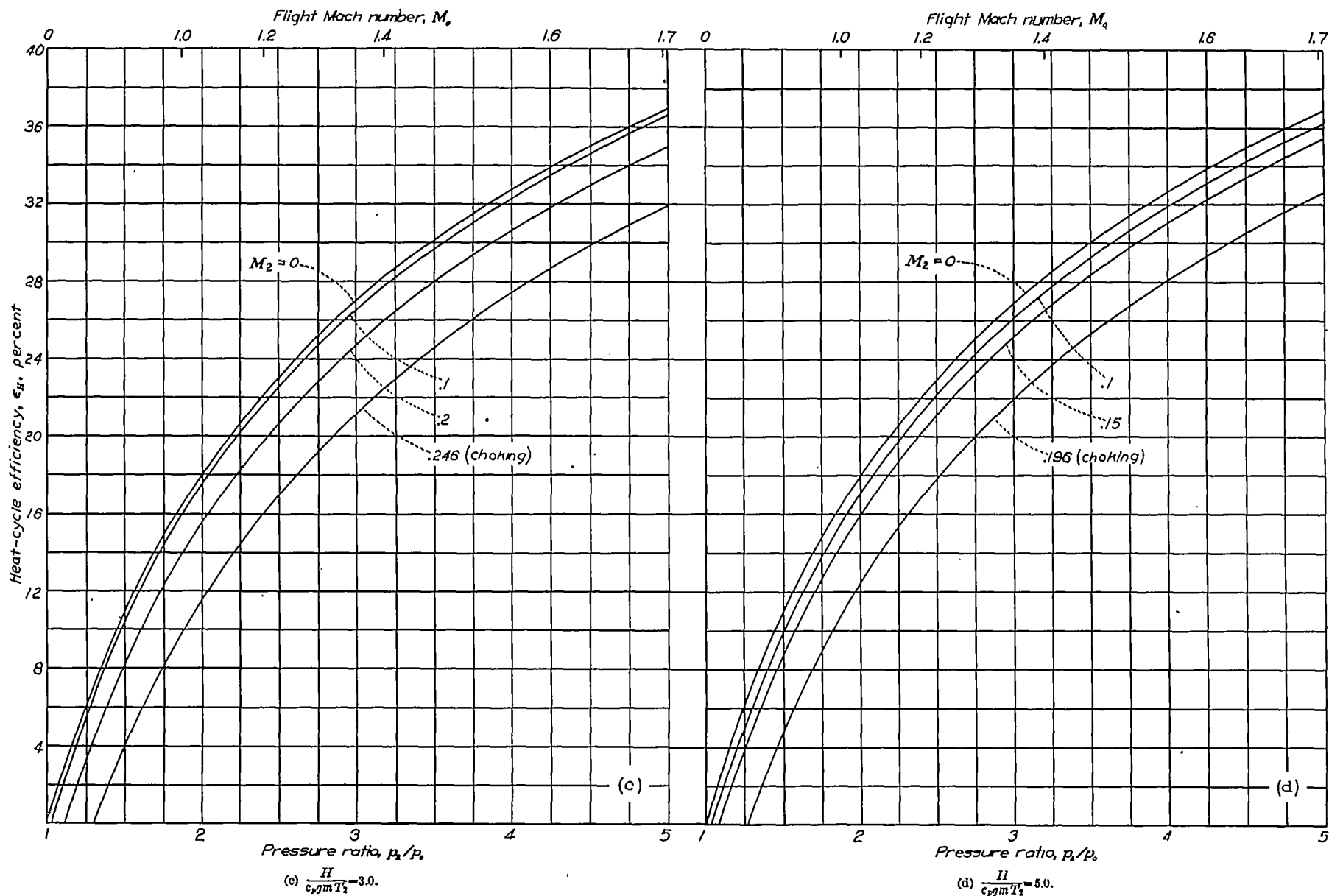


FIGURE 8.—Concluded.

The Mach number at the entrance to the combustion chamber,  $M_2$ , is shown in figure 8 to have a large effect on the heat-cycle efficiency. When  $M_2$  is very small, approaching zero in value, the heat-cycle efficiency approaches the value given by equation (35), regardless of the heating rate. As  $M_2$  increases, however, the value of  $\epsilon_H$  decreases because of the pressure drop due to acceleration of the heated air in the combustion chamber. For a given value of  $M_2$ , increasing the rate of heating causes decreases in  $\epsilon_H$  for the same reason. The limiting or "choking" values of  $M_2$  are also shown in figure 8. If no heat were added, the highest possible value of  $M_2$  would be 1.0. As heat is added, the choking value of  $M_2$  decreases because sonic velocity is reached at the end of the combustion chamber ( $M_3=1.0$ ) for values of  $M_2$  less than 1.0. At the high rates of heating (for example, at  $\frac{H}{c_p g m T_2} = 5.0$ , which corresponds to a temperature rise of the order of 2500° F in the combustion chamber), the choking value of  $M_2$  becomes very small, only 0.196 for the example cited. This effect is extremely important because it dictates the minimum possible area expansion  $A_2/A_0$  for a given heating rate.

The flight Mach numbers required to produce the compression ratios of figure 8 (assuming ideal stagnation pressure is obtained at station 2) are noted on the figure. At the higher supersonic speeds, the ideal thermal efficiencies for low values of  $M_2$  approach those obtainable in internal-combustion engines. This result would be expected in view of the fact that the compression ratios are of comparable magnitude.

Because  $\epsilon_H$  increases with compression ratio, the inlet ducting and diffuser losses should be as low as possible. If an internal blower is not used, high pressures in the heating section of the duct can be obtained only when the area of this section is greater than the initial area  $A_0$  of the internal-flow tube. (See fig. 2.) This location of the heating device in a high-pressure, low-velocity section of the duct is also ideal from the standpoint of minimizing the losses in the heating device.

The friction loss within the heating device,  $\Delta h_r$ , has the undesirable effect of reducing the compression ratio. For reasons of simplification this loss was neglected in the evaluation of  $\epsilon_H$ , equation (37), figure 8. If the principal part of this loss occurs upstream from the region in which heat is added, it may be accounted for by using  $p_2 - \Delta h_r$  instead of  $p_2$  as the effective pressure at the entrance to the heating region. In the case in which the friction loss is intimately involved in the heating process as in a tubular radiator, the actual pressure drop during heating will be greater than assumed in equation (37). As an approximation for a combustion chamber, it may be assumed that the effective pressure is  $p_2 - \frac{\Delta h_r}{2}$

at the entrance to the chamber, and this value may then be used in equation (37) or figure 8 to obtain  $\epsilon_H$ . In both of these examples, the value of  $\Delta h_r$  should include estimates of the heating and compressibility effects on the friction loss

if low-speed data for unheated devices are used in the calculation.

Calculation of the net internal drag (or thrust).—In performance studies, it is desirable to compute the resultant drag, or thrust, due to the heated internal flow without going through the step-by-step duct calculations previously discussed. The method to be described is exact within the limits of the assumption that the outlet flow is uniform. Very few steps and only simple slide-rule operations are involved.

The net force due to the internal flow (equation (21)) is

$$D = m(V_0 - v_6) = m(V_0 - v_6') - m(v_6 - v_6') \quad (38)$$

Equation (29) shows the significance of the two terms of equation (38) to be:

$$\begin{aligned} (\text{Net force due to internal flow}) = & (\text{Internal drag} \\ & \text{without heat}) - (\text{Drag reduction due to heating}) \end{aligned}$$

Each of these components can be computed without difficulty, and the separation of the two is the basis for the present method.

If the flow were incompressible, the drag corresponding to the unheated condition could be very easily computed from

$$D_i' = m(V_0 - v_{6i}') = m \left[ V_0 - \left( V_0^2 - \frac{\Delta h}{\rho_0/2} \right)^{1/2} \right]$$

or

$$C_{D_i}' = \frac{D_i'}{q_0 F} = 2C \left[ 1 - \left( 1 - \frac{\Delta h}{q_0} \right)^{1/2} \right] \quad (39)$$

where  $\Delta h/q_0$  is obtained from equation (23) for values of mass-flow coefficient and radiator drag corresponding to the heated-flow condition. For compressible flow, unfortunately, the drag calculation is laborious. A relation exists, however, between the true value of  $C_D$  for compressible flow and the value computed from the simple incompressible-flow formula, equation (39). From equations (21) and (39),

$$\left( \frac{C_D}{C_{D_i}'} \right)' = \frac{1 - \frac{v_6}{V_0}}{1 - \sqrt{1 - \frac{\Delta h}{q_0}}}$$

This equation involves only the total-pressure loss  $\Delta h/q_0$  and the velocity ratio  $v_6/V_0$ , which can be defined in terms of  $\Delta h/q_0$  and  $M_0$  from equations presented in appendix B. A plot of this relation is given in figure 9 and may be used to obtain the true value of the internal drag for the unheated condition using the value of the low-speed drag coefficient computed from equation (39); that is,

$$C_D' = C_{D_i}' \left( \frac{C_D}{C_{D_i}'} \right)'$$

the quantity  $\left( \frac{C_D}{C_{D_i}'} \right)'$  being taken from figure 9.

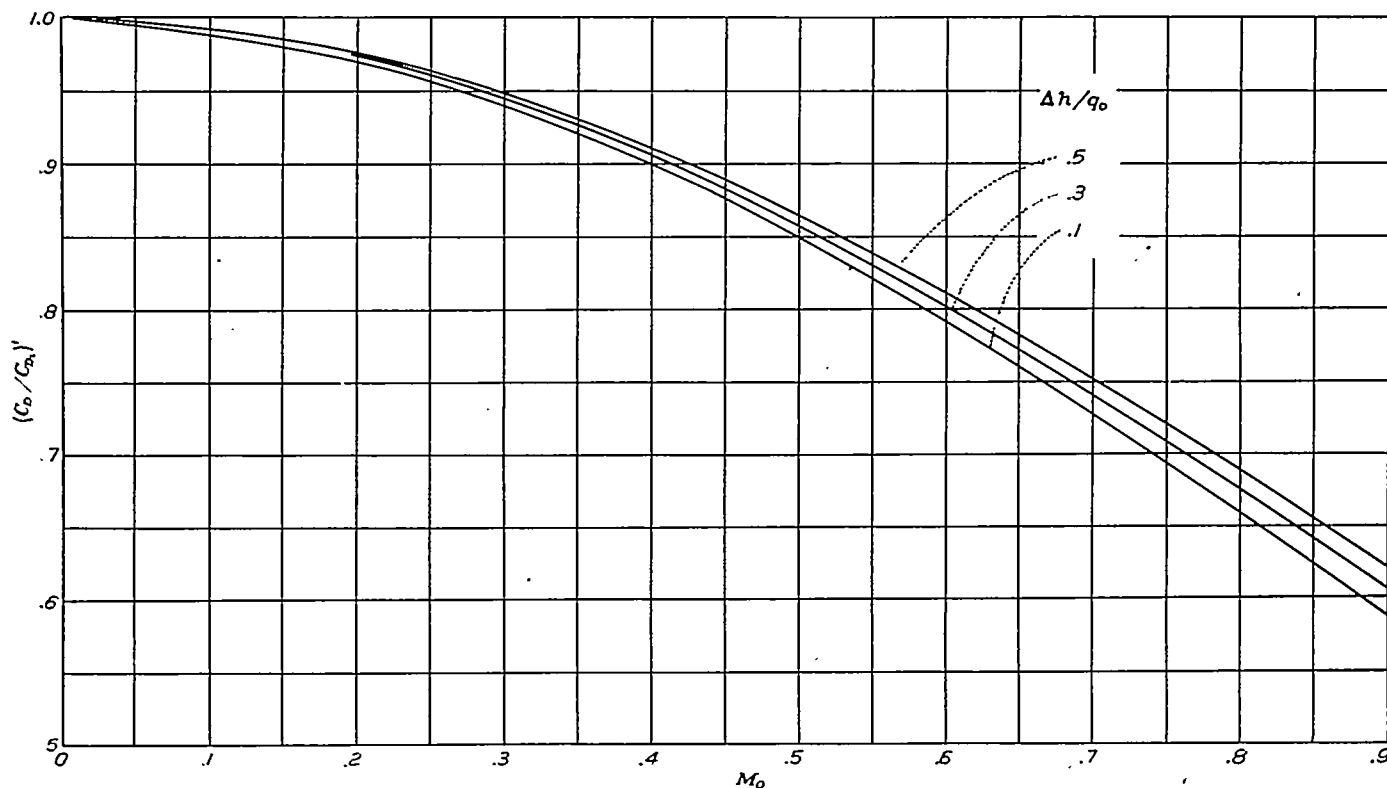


FIGURE 9.—Ratio of the internal-drag coefficient for compressible flow to the value computed for incompressible flow as a function of Mach number.

The drag for the unheated condition having been already obtained, only the drag reduction due to heating (second term of equation (38)) remains to be computed. From equations (32) and (33) the drag reduction, or thrust, due to heating is

$$\Delta D = -\frac{\epsilon_H \epsilon_M JH}{V_0}$$

or

$$\Delta C_D = -\frac{\epsilon_H \epsilon_M JH}{q_0 F V_0} \quad (40)$$

In summary, the net or resultant force (taken as positive in the drag direction) is given by the following formula:

$$C_D = C_{D'} - \Delta C_D = 2C \left[ 1 - \left( 1 - \frac{\Delta h}{q_0} \right)^{1/2} \right] \left( \frac{C_D}{C_{D_i}} \right)' - \frac{JH}{q_0 F V_0} \epsilon_H \epsilon_M \quad (41)$$

in which the parameters involved are computed as follows:

- $\Delta h/q_0$  equation (23)
- $(C_D/C_{D_i})'$  from figure 9
- $\epsilon_H$  from figure 8 or equation (35) or (37)
- $\epsilon_M$  from equations (34) and (41) by trial

The separation of the propulsive effect of heating from the internal drag due to frictional effects is useful in several other connections. In the correction of wind-tunnel data obtained without heat, for example, the right-hand term of equation (41) may be used to evaluate the drag reduction due to heating. It is obvious that model tests should be made with values of  $\Delta h/q_0$  and  $C$  corresponding to the heated condition. A further application of the separation principle will be made in part II, where the thrust force due

to the added heat is separated from the net force due to the internal flow. The results analyzed on this basis are significant as applied to any internal system.

## II. HIGH-SPEED WIND-TUNNEL TESTS OF A MODEL RAM-JET PROPULSION SYSTEM APPARATUS AND METHODS

The Langley 8-foot high-speed wind tunnel, in which these tests were carried out, is a closed-throat, circular-section, single-return tunnel with airspeed continuously controllable for speeds from about 75 to 600 miles per hour. The turbulence of the air stream is unusually low but is somewhat higher than in free air.

The model tested consisted of a 13.6-inch-diameter body of revolution housing a 160-kilowatt heating device and mounted on a 9-percent-thick, 20-inch-chord, low-drag airfoil that spanned the jet (fig. 10). The air inlet was at the nose of the body with an expanding duct section back to the radiator. The air outlet was at the tail. The general model layout is shown in figure 11 with the ordinates listed in tables I and II.

The external shape of the wing-fuselage combination was designed to have a critical speed in excess of the maximum test speed. In order to meet this criterion, inlet and outlet openings designed according to reference 4 were utilized, and a 9-percent-thick 20-inch-chord wing of airfoil section NACA 66-009 was required. The inlet- and outlet-opening shapes of reference 4 had the further advantage of permitting wide variations in the rate of internal flow and in the inlet- and outlet-velocity ratios without causing appreciable external-drag changes.

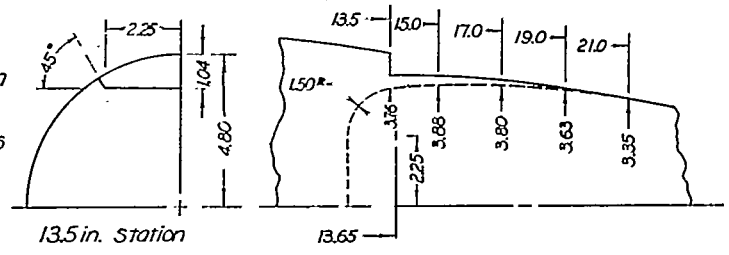


FIGURE 10.—Model assembly

| x    | y    | x     | y    |
|------|------|-------|------|
| 0    | 0    | 8.00  | .688 |
| .10  | .139 | 9.00  | .699 |
| .15  | .167 | 10.00 | .697 |
| .25  | .209 | 11.00 | .681 |
| .50  | .282 | 12.00 | .642 |
| 1.00 | .389 | 13.00 | .782 |
| 1.50 | .469 | 14.00 | .691 |
| 2.00 | .535 | 15.00 | .568 |
| 3.00 | .638 | 16.00 | .444 |
| 4.00 | .718 | 17.00 | .319 |
| 5.00 | .782 | 18.00 | .185 |
| 6.00 | .832 | 19.00 | .074 |
| 7.00 | .866 | 20.00 | 0    |

Leading-edge radius = 0.112

Fuselage ordinates given in tables I and II  
All dimensions in inches



Partial-annular outlet, tail E

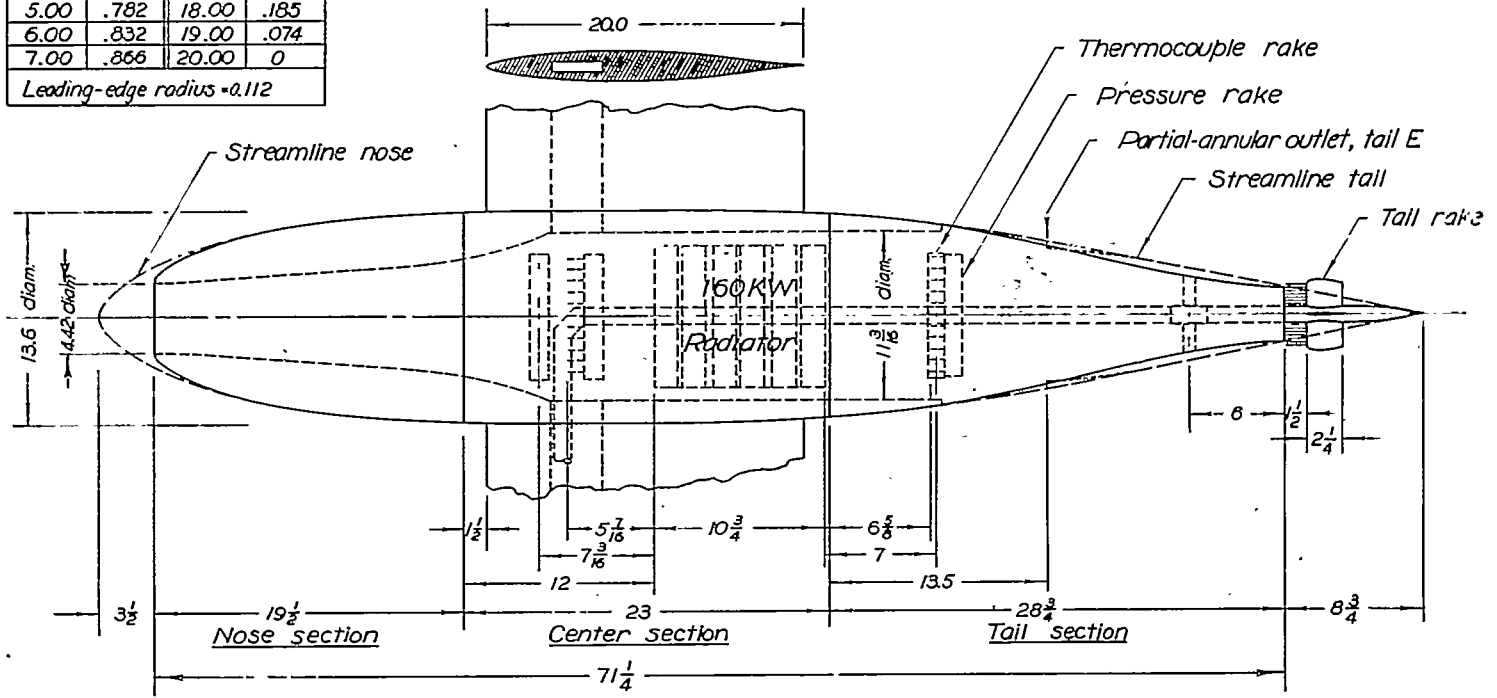


FIGURE 11.—Model details.

TABLE I.—STREAMLINE-BODY ORDINATES IN INCHES

| Streamline nose |      | Center section |      | Streamline tail |      |
|-----------------|------|----------------|------|-----------------|------|
| x               | R    | x              | R    | x               | R    |
| 0               | 0    | 0              | 6.78 | 0               | 6.49 |
| .73             | 1.29 | 1.5            | 6.80 | 3.0             | 6.25 |
| 1.46            | 1.95 | 4.5            | 6.80 | 6.0             | 5.92 |
| 2.92            | 2.93 | 10.5           | 6.80 | 9.0             | 5.52 |
| 4.37            | 3.64 | 13.5           | 6.80 | 12.0            | 5.06 |
| 5.83            | 4.21 | 15.5           | 6.78 | 15.0            | 4.52 |
| 8.73            | 5.03 | 18.5           | 6.71 | 18.0            | 3.94 |
| 11.66           | 5.64 | 21.5           | 6.58 | 21.0            | 3.35 |
| 14.58           | 6.10 | 23.0           | 6.40 | 24.0            | 2.75 |
| 17.49           | 6.44 |                |      | 27.0            | 2.14 |
| 20.41           | 6.67 |                |      | 30.0            | 1.53 |
| 23.00           | 6.78 |                |      | 33.0            | .92  |
|                 |      |                |      | 37.5            | 0    |

Three cusped-type openings at the tail (figs. 10 and 11) were employed to vary the internal mass-flow coefficient *C* from about 0.07 for the largest size (tail A) to about 0.025 for the smallest size (tail C). Tail D was similar in size to the intermediate cusped outlet (tail B) but had straight, slightly converging walls. Tail E was a partial-annular outlet located at the 56-inch station on the body and designed according to reference 7. Tails B, D, and E had approximately the same flow coefficient, namely, 0.052.

TABLE II.—DUCTED-BODY ORDINATES IN INCHES

| Diffuser |      | Ducted body nose ordinates |      | Tail         | A     | B     | C     |
|----------|------|----------------------------|------|--------------|-------|-------|-------|
| x        | R    | x                          | R    | x            | R     | R     | R     |
| 0        | 2.34 | 0                          | 2.34 | 0            | 6.49  | 6.49  | 6.49  |
| .10      | 2.21 | .025                       | 2.44 | 3.00         | 6.25  | 6.25  | 6.25  |
| .25      | 2.21 | .05                        | 2.70 | 6.00         | 5.92  | 5.91  | 5.88  |
| .50      | 2.21 | .10                        | 2.58 | 9.00         | 5.47  | 5.42  | 5.37  |
| .75      | 2.22 | .25                        | 2.75 | 12.00        | 4.89  | 4.80  | 4.71  |
| 1.00     | 2.23 | .50                        | 2.98 | 15.00        | 4.24  | 4.09  | 3.90  |
| 1.75     | 2.28 | .75                        | 3.16 | 18.00        | 3.57  | 3.37  | 3.18  |
| 7.75     | 2.69 | 1.00                       | 3.33 | 21.00        | 2.95  | 2.70  | 2.40  |
| 14.75    | 3.17 | 1.75                       | 3.73 | 24.00        | 2.42  | 2.7   | 1.87  |
| 16.75    | 3.34 | 2.75                       | 4.15 | 27.00        | 2.07  | 1.82  | 1.48  |
| 18.75    | 3.59 | 3.75                       | 4.49 | 28.75        | 1.985 | 1.705 | 1.365 |
| 20.75    | 3.98 | 4.75                       | 4.79 |              |       |       |       |
| 22.75    | 4.58 | 6.75                       | 5.29 |              |       |       |       |
| 25.00    | 5.59 | 8.75                       | 5.71 | Outlet diam. | 3.92  | 3.30  | 2.68  |
|          |      | 10.75                      | 6.04 |              |       |       |       |
|          |      | 12.75                      | 6.30 |              |       |       |       |
|          |      | 14.75                      | 6.51 | Outlet area  | 11.07 | 7.88  | 4.04  |
|          |      | 16.75                      | 6.66 |              |       |       |       |
|          |      | 18.75                      | 6.76 |              |       |       |       |
|          |      | 19.00                      | 6.78 |              |       |       |       |

The internal system was designed to house the radiator and survey equipment with a minimum of duct losses. A more detailed description of the model and design considerations is given in reference 5.

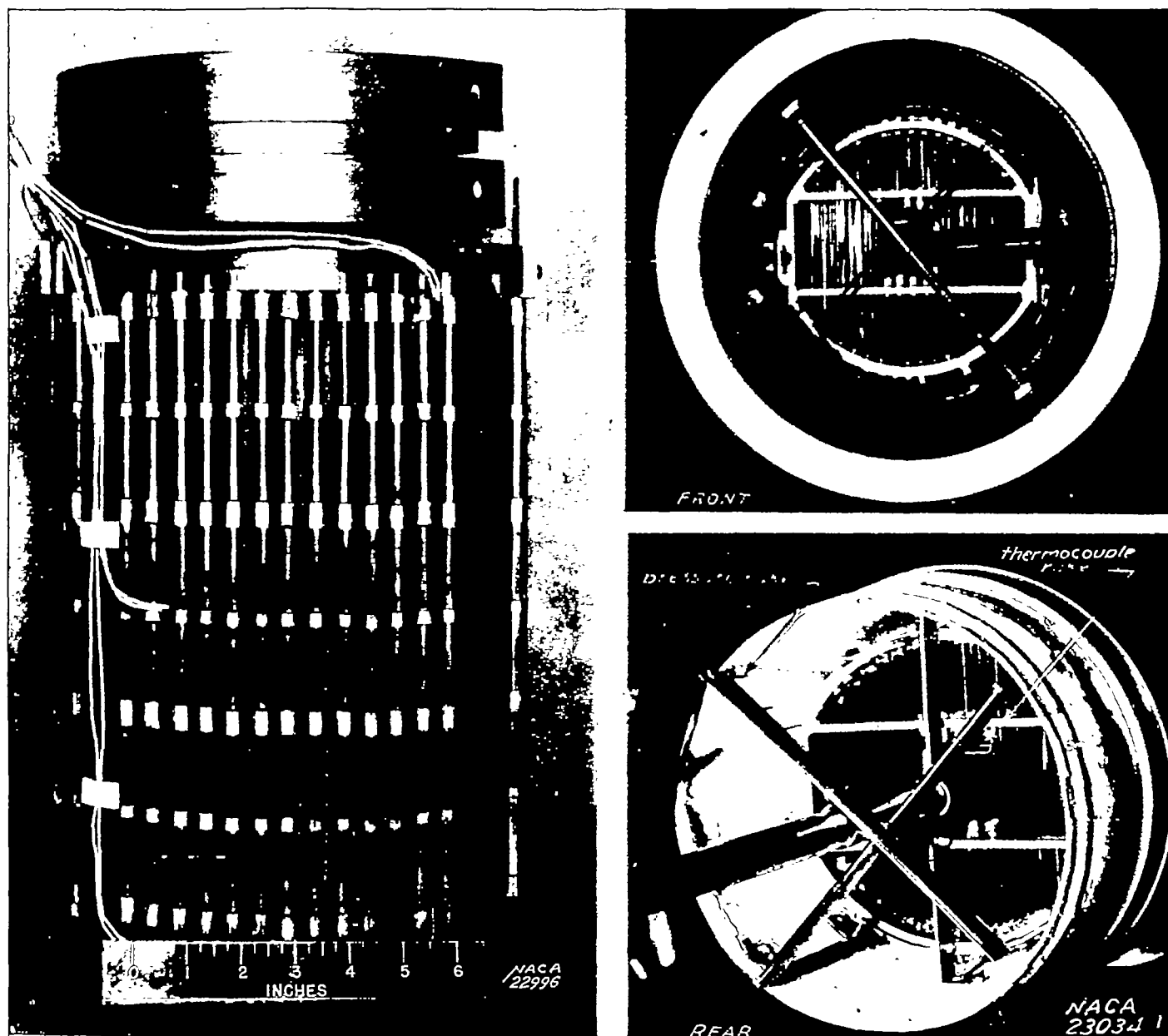


FIGURE 12.—Radiator details and installation.

## RADIATOR

The heat input to the internal air flow was provided by a 160-kilowatt, 220-volt, three-phase electric resistance radiator designed for a maximum operating temperature of 1500° F. The radiator consisted of six elements of 1½ inch × 0.020 Nichrome V furnace strip (radiating surface, 32 sq ft) woven on a framework of reinforced asbestos millboard supports (figs. 12 and 13). Radiator temperature was measured by four chromel-alumel thermocouples welded to the elements.

Power input to the radiator was controlled by eight transformer voltage taps spaced to provide approximately uniform power increments. Total power input was measured by a standard three-phase wattmeter.

## SURVEY EQUIPMENT

**Pressure surveys.**—Pressures ahead of and behind the radiator were measured, respectively, by an 8-tube and an 11-tube static- and total-pressure rake spanning the duct. (See figs. 11 and 12 for installation details.) All pressure tubes were connected to a standard manometer and the pressure readings were photographically recorded. A 52-tube removable survey rake of static- and total-pressure tubes was installed at station 4 for measurement of the internal and external pressures at the tail outlet. The rake tubes were supported by two 2¼-inch-chord blades (NACA section 16-010) set at right angles to each other and extending beyond the outlet walls (fig. 14). The tail rake was supported by a 1½-inch outside-diameter steel tube housing the pressure leads and extending through the core of the radiator to the wing duct (fig. 11).

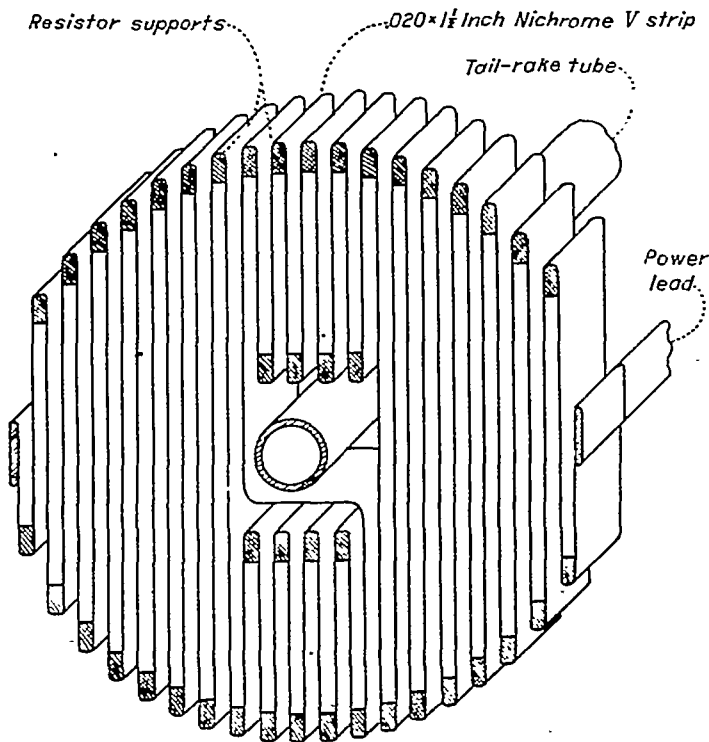


FIGURE 13.—Radiator element.

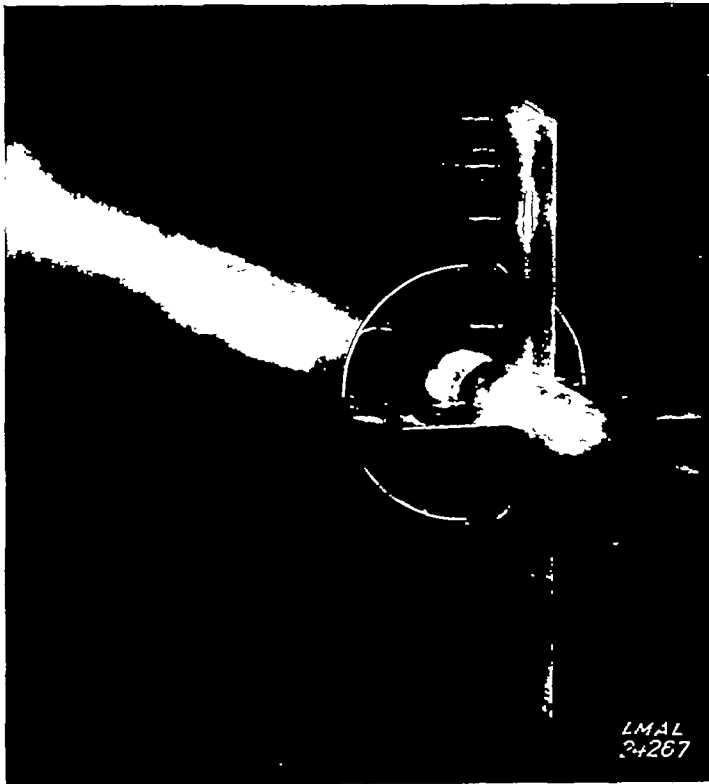


FIGURE 14.—Tail-rake installation.

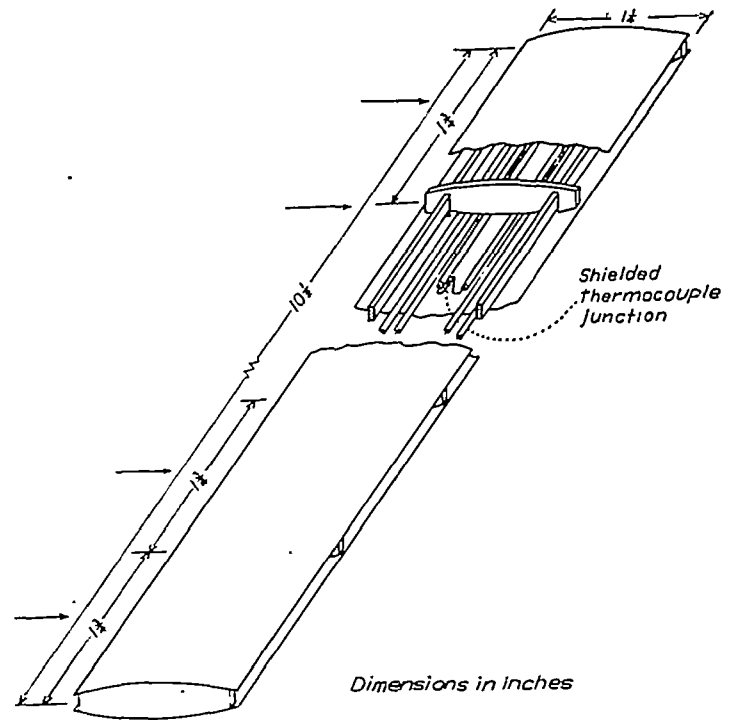


FIGURE 15.—Thermocouple rake.

**Temperature measurements.**—All temperatures were measured by calibrated thermocouples connected to a sensitive potentiometer. Air temperature ahead of the radiator was measured by two shielded thermocouples located in the front thermocouple rake. (See fig. 15 for rake details.)

Shielding of the junction prevented false air-temperature readings due to radiation effects. Air-temperature rise across the radiator was measured directly by two thermocouple rakes containing six junctions in separate compartments (fig. 15). The thermocouples in the front rake were the cold junctions and the corresponding thermocouples in the rear rake were the hot junctions.

**Temporary apparatus.**—During preliminary calibration runs, additional apparatus was installed in the model to supplement the fixed equipment. A 14-tube total-pressure rake spanning the duct was mounted behind the radiator to aid in determining the duct velocity profile. From these data the energy added to the air stream was determined by an integration of the mass flow and the air-temperature rise.

The heat lost through the walls of the tail was computed from measurements of the wall temperatures and local skin-friction coefficients. A standard 5-tube static- and total-pressure "mouse" was used to survey the boundary layer of tail B in conjunction with local wall-temperature measurements by thermocouples.

#### TESTS

Drag tests with each outlet were carried through a Mach number range of 0.26 to 0.75 (approx. 200 to 560 mph in the 8-ft. high-speed tunnel). The tail rake (fig. 14) was removed

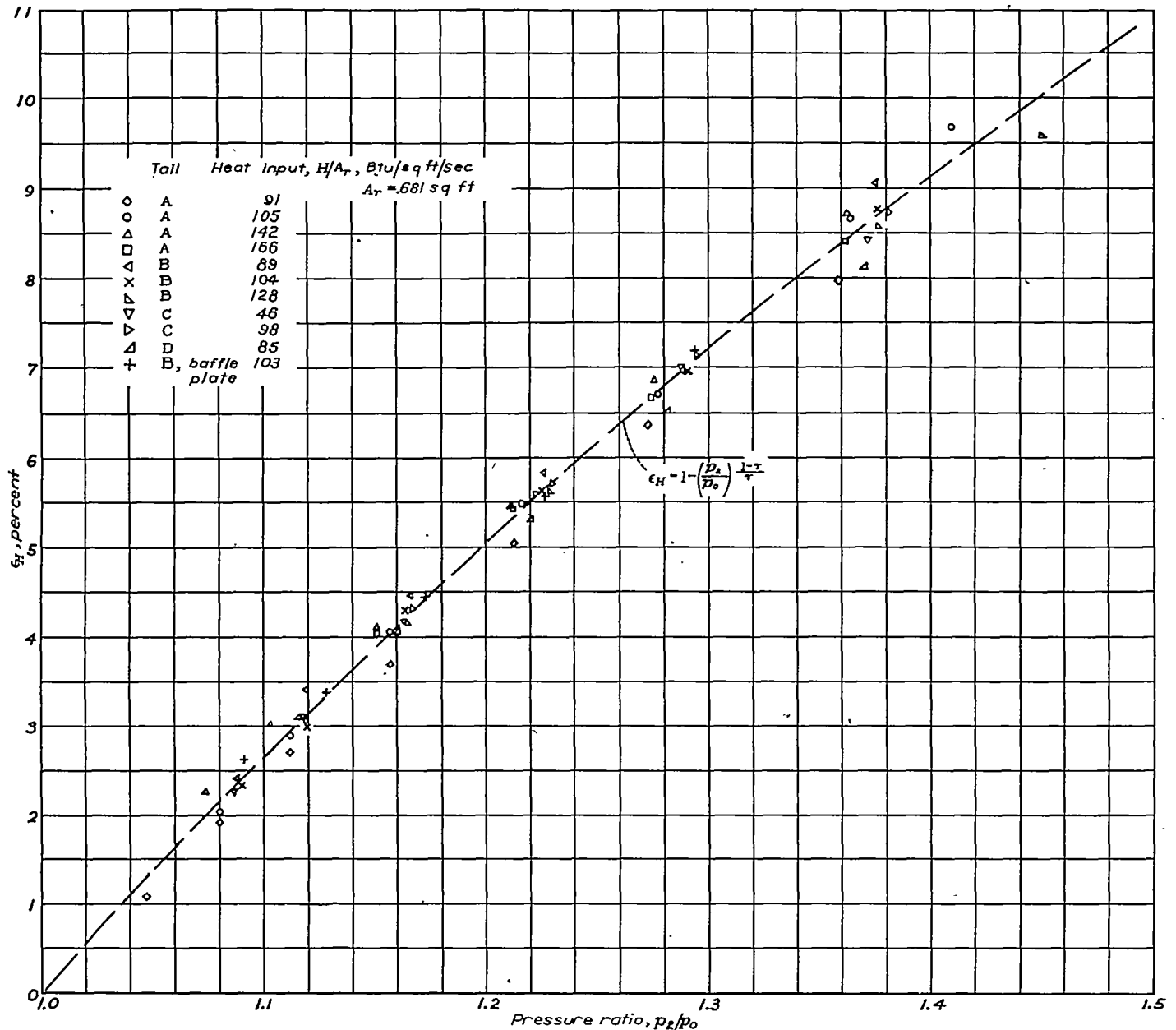


FIGURE 16.—Variation of heat-cycle efficiency with pressure ratio for various heat inputs. Data from pressures at outlet.

during the force tests. Internal pressures at stations 2 and 3 were recorded simultaneously with the force data, as was the power input to the radiator. The range of power input was from 0 to 160 kilowatts.

Tests of the model with the tail outlets A, B, C, and D were made with the tail rake (fig. 14) in place and were similar in range to the force tests. The object of these runs was to furnish data for calculations of the heat-energy recovery independent of force measurements and also to evaluate external-drag changes under various heating conditions. A special run was made with tail B with an internal resistance plate that produced a total-pressure drop of  $0.27q_0$ .

Supplementary runs to permit an estimation of the heat lost through the walls included measurements of wall temperature and boundary-layer velocity profiles.

All tests were made at zero angle of attack.

#### RESULTS

The methods employed to compute the heat-cycle efficiency and the duct-flow characteristics from the test data are described in appendix B.

Figure 16 shows the variation of heat-cycle efficiency with compression ratio as determined from the wake-survey data. The experimental results are shown for all the tests and therefore cover a wide range of mass-flow rates, heat input, Mach

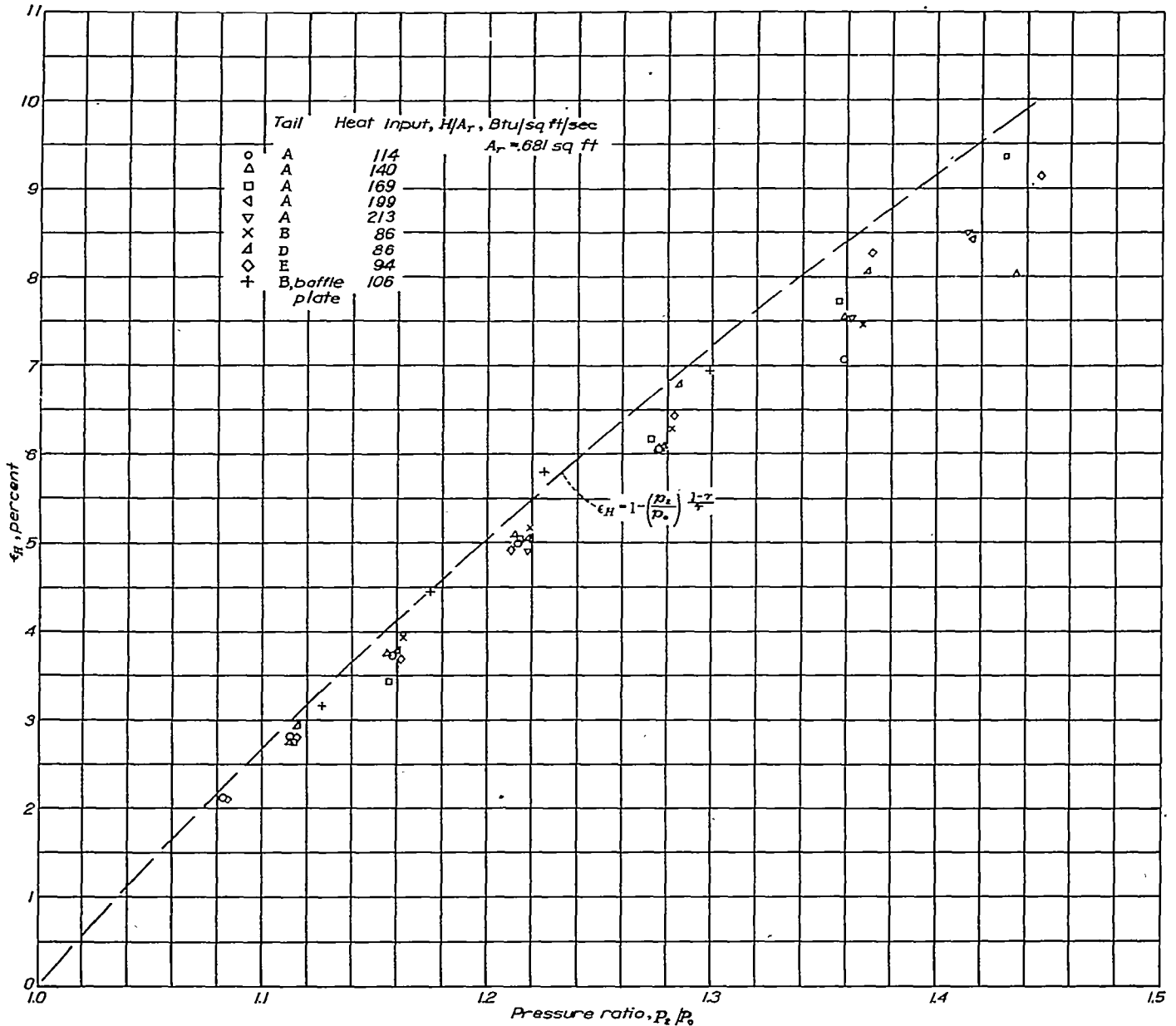


FIGURE 17.—Variation of heat-cycle efficiency with pressure ratio for various heat inputs. Data from force measurements.

number, and ducting losses. The heat-cycle efficiency indicated by the force-test data is shown on figure 17 for the same range of variables as presented for the pressure measurements.

Comparisons of the flow characteristics measured at key stations in the duct with the characteristics computed by the methods of part I are shown in figure 18. Table III shows a comparison of the test values of total-pressure loss with the corresponding values computed from the theory. Table IV shows a comparison of experimental and theoretical mass-flow ratios. Figure 19 compares the experimental variation of mass-flow coefficient with outlet density ratio with the variations computed from the simplified theory (equation (27)) presented in part I.

DISCUSSION

Efficiency of heat-recovery process.—The maximum Mach numbers of the duct flow at the radiator section did not exceed 0.10. Reference to figure 8 or to equation (37) will

show that, for this low value of  $M_2$ , the heat-cycle efficiency depends only on the compression ratio  $p_2/p_0$ ; that is,

$$\epsilon_H = 1 - \left(\frac{p_2}{p_0}\right)^{\frac{1-\gamma}{\gamma}}$$

TABLE III.—COMPARISON OF EXPERIMENTAL AND THEORETICAL VALUES OF TOTAL-PRESSURE LOSS

[Tail B, baffle plate]

| M     | Total-pressure loss, $\Delta h/q_0$ |              |               |              |
|-------|-------------------------------------|--------------|---------------|--------------|
|       | H=0                                 |              | H=90 Btu/sec  |              |
|       | Equation (23)                       | Experimental | Equation (23) | Experimental |
| 0.263 | 0.299                               | 0.301        | -----         | -----        |
| .347  | .299                                | .298         | -----         | -----        |
| .403  | .298                                | .296         | 0.218         | 0.228        |
| .473  | .294                                | .294         | .225          | .232         |
| .545  | .290                                | .292         | .233          | .235         |
| .615  | .286                                | .289         | .236          | .237         |
| .689  | .282                                | .286         | .238          | .239         |

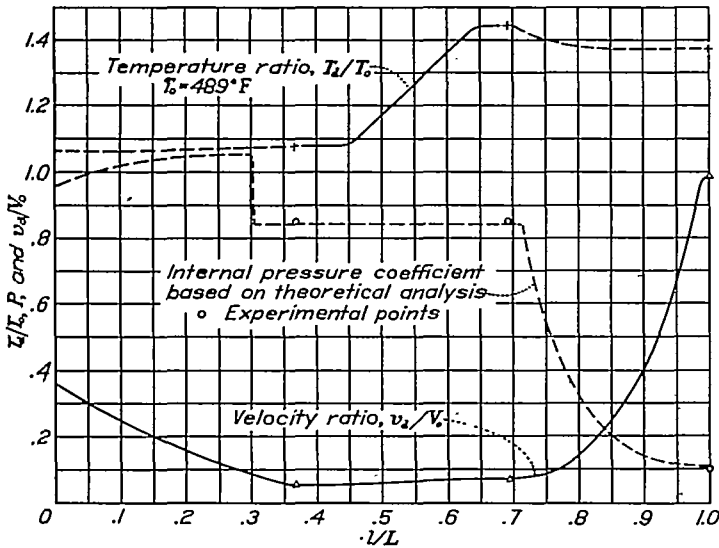


FIGURE 18.—Temperature ratio, Internal pressure coefficient, and velocity ratio for tail B at  $M=0.615$ . Heat input, 63.2 Btu per square foot per second.

This relation is shown for comparison with the experimental data obtained from the wake pressure surveys in figure 16. Virtually all of the heat energy theoretically recoverable was actually recovered. The data shown represent a very wide range of heating conditions and internal mass-flow rates. The maximum air-temperature rise in the tests was about 300° F and the flow coefficient  $C$  varied from about 0.025 to 0.070.

The recovery process was not measurably affected by any increase in ducting loss due to heating because of the extremely low initial value of the ducting loss for the model tested. With tail B, the medium-size outlet, the loss across the radiator was only  $0.008q_0$  and the loss in the converging duct behind the radiator was about  $0.007q_0$  for a mass-flow coefficient of 0.050.

The heat loss through the walls between the radiator and the tail outlet is estimated as approximately 1 percent of the heat added. The heat loss determined from the wall-temperature and boundary-layer surveys agreed with the theoretical calculations of this loss. Allowance for this small correction was made in the reduction of the data, but there was no measurable change in the recovery process with so small a heat loss.

The force measurements of the net thrust caused by heating provided a means of determining a value of  $\epsilon_H$

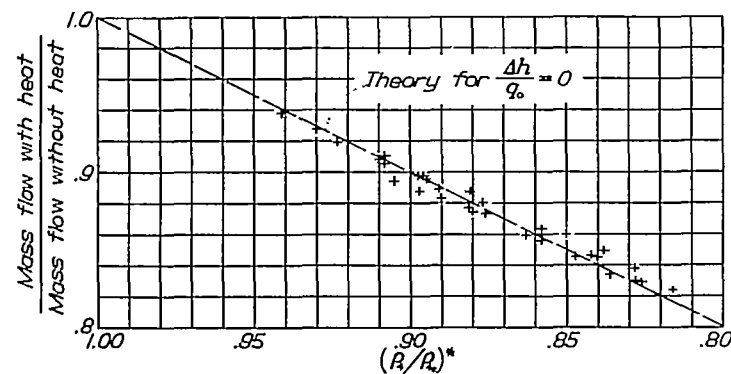


FIGURE 19.—Variation of internal mass flow with outlet density ratio.

that includes the external losses associated with exhausting the hot air of increased velocity. This value of  $\epsilon_H$  is shown in figure 17. As noted from the definition of  $\epsilon_H$  (see equations (31) and (33)), the over-all efficiency given by the force tests was reduced by the mechanical or Froude efficiency factor  $\epsilon_M$  in computing  $\epsilon_H$ . The force-test data closely approach the ideal value of  $\epsilon_H$ . The results are consistent, however, in indicating small losses. Comparison of figures 16 and 17 leads to the conclusion that the losses must be due to slight increases in external drag from the heated exhaust flow.

TABLE IV.—COMPARISON OF EXPERIMENTAL AND THEORETICAL VALUES OF MASS-FLOW RATIO

(Tail B, baffle plate)

| M     | Mass-flow ratio, $\rho v_1 / \rho_0 V_0$ |               |              |               |               |              |
|-------|--|---------------|--------------|---------------|---------------|--------------|
|       | H=0                                      |               |              | H≈90 Btu/sec  |               |              |
|       | Equation (27)                            | Equation (26) | Experimental | Equation (27) | Equation (26) | Experimental |
| 0.263 | 0.767                                    | 0.778         | 0.772        | -----         | -----         | -----        |
| .347  | .767                                     | .788          | .781         | -----         | -----         | -----        |
| .403  | .767                                     | .790          | .786         | 0.621         | 0.675         | 0.672        |
| .473  | -----                                    | -----         | -----        | .639          | .696          | .694         |
| .545  | -----                                    | -----         | -----        | .657          | .719          | .718         |
| .615  | -----                                    | -----         | -----        | .668          | .734          | .736         |
| .689  | .767                                     | .828          | .819         | .676          | .761          | .756         |

Measurements of the external drag with the tail rake were made in only the vertical plane (fig. 14). The results so obtained showed no consistent external-drag changes with heating. In any case, such changes in external drag were very small; a 1-percent change in the drag of the body would account for the small divergence between the ideal and the measured efficiency at the highest test speed and heat input.

The heated flow from the annular outlet had as little effect on the external drag as did that from the tail outlets. This result does not seem surprising when it is considered that the dynamic pressure in the heated flow was virtually equal to that of the cold outlet flow. The increased velocity is offset by the decreased density so that there is little change in  $\frac{1}{2} \rho v_1^2$  and correspondingly little change in external drag.

(See part I.)

The efficiencies obtained with the duct pressure reduced by  $0.27q_0$  by means of the baffle plate approached the predicted efficiency for the measured compression ratio as closely as in the runs with low internal losses.

Figures 16 and 17 indicate that the use of the ideal relation for the heat-cycle efficiency is justified for design calculations. If the duct-flow Mach number  $M_2$  is low, say less than 0.10, the heat-cycle efficiency is adequately given by the simple relation of equation (35),

$$\epsilon_H = 1 - \left( \frac{p_2}{p_0} \right)^{\frac{1-\gamma}{\gamma}}$$

Otherwise, the more exact relation (equation (37)) must be employed, in which case  $\epsilon_H$  may be obtained for the particular values of  $M_2$  and  $\frac{H}{c_p g m T_2}$  involved.

The data accumulated in the tests are useful in verifying the relations, developed in part I, concerning the calculation of the flow characteristics at key stations in the duct, the effects of heat on the over-all flow characteristics, and the net propulsive force. Comparison of the computed and the measured values of these characteristics will now be made in the foregoing order.

Comparison of calculated and measured internal-flow characteristics.—The internal-flow characteristics at the key stations in the duct were computed from the equations of part I on the basis of the following constants, which correspond to one of the test conditions with tail B:

|   |          |
|---|----------|
| $H$ , Btu per second.....                                     | 68.2     |
| $V_0$ ,<br>miles per hour.....                                | 456      |
| feet per second.....  | 669      |
| $p_0$ , pounds per square foot.....                           | 1653     |
| $\rho_0$ , slug per cubic foot.....                           | 0.001970 |
| $C_{D_i}$ .....   | 75       |
| $(\Delta h/q_0)_{\text{duct}}$ , including diffuser loss..... | 0.03     |
| $\eta_d$ .....  | 0.93     |
| $P_1$ .....   | 0.11     |
| $A_1$ (outlet area), square foot.....                         | 0.0547   |

The computed mass-flow coefficient is 0.0399, as compared with the measured value, 0.0401. The area,  $A_0=0.0403$  square foot, which corresponds to the computed mass-flow coefficient, was used in calculating the pressure, the temperature, and the velocity at each station in the duct according to the equations of part I. The results are compared with the measured data in figure 18 and show that the flow characteristics of an efficient system, in which the velocity distribution is fairly uniform, can be computed with good accuracy.

Effects of heat and compressibility on the internal total-pressure loss.—Table III gives a comparison of the measured variations of total-pressure loss for the tests with the internal resistance plate with the results computed by equation (23). Two rates of heating and a range of values of Mach number are shown. The reduction of the total-pressure loss with increased heating is due to the decrease in internal mass flow accompanying the addition of heat. For a given rate of heating, the total-pressure loss decreases as the Mach number  $M_0$  increases in systems with a fixed outlet size. This result is caused by the appreciable increase in density of the air at the radiator section of the duct as the Mach number increases. With a given outlet opening and fixed rate of heating, the mass-flow coefficient does not change greatly as the Mach number advances; the increased density at the radiator section therefore resulted in decreased velocity ratios through the radiator and in correspondingly decreased radiator losses. It will be noted from table III that equation (23) predicts both the effects of heating and of Mach number very accurately.

Effects of heat and compressibility on the internal mass-flow rate.—As shown by equation (26), the mass flow through a system with a given outlet area will be reduced in proportion to the square root of the outlet density, provided that the internal losses are negligible. Figure 19 compares this theoretical variation with the experimental

results for all of the tests except the runs with the added internal resistance. The agreement is excellent. For these tests, the decrease in mass-flow rate was independent of Mach number for a Mach number range from 0.26 to 0.75.

When an appreciable internal total-pressure loss is present, as in most practical installations, the change in mass-flow rate no longer varies simply as  $\rho_1^{1/2}$  but depends on both the internal resistance and on the Mach number  $M_0$ . Table IV shows the flow variation obtained experimentally with the resistance plate in the duct and, for comparison, the flow variations computed by equation (26) and also by the approximate equation (27). The exact equation (equation (26)) agrees very closely with the experimental results, but equation (27) departs appreciably from the experimental values at the higher Mach numbers. It has been found, however, that the approximate equation (27), which does not account for Mach number changes, yields sufficiently accurate results at Mach numbers below about 0.30.

With an appreciable internal loss, the reduction in mass-flow rate with heating is less than the reduction indicated by the  $\rho_1^{1/2}$  relation. The reduced total-pressure loss accompanying the addition of heat in a system with a fixed outlet opening tends to increase the internal flow and this effect nullifies to some extent the throttling effect of the heat.

Computation of the net force due to the heated internal flow.—An example of the simple method described in part I for computing the net force will now be given. The same duct characteristics and the same initial conditions assumed in the preparation of figure 18 will be used. In addition to the flow characteristics previously listed, the total-pressure loss  $\frac{\Delta h}{q_0}=0.238$  and the compression ratio  $\frac{p_2}{p_0}=1.226$  are re-

quired. These values were computed from the basic data.

The low-speed drag coefficient without heat is (from equation (39))

$$C_{D_i}' = 2 \times 0.0401 (1 - \sqrt{1 - 0.238}) = 0.0103$$

The drag coefficient without heat but at the design Mach number  $M_0=0.615$  is (from fig. 9)

$$C_{D'} = 0.0103 \times 0.790 = 0.0081$$

From equation (35) (or fig. 8 for  $M_2 \approx 0$ ), the efficiency of the heat cycle is

$$\epsilon_H = 1 - (1.226)^{-0.238} = 0.0565$$

The drag reduction due to heating is given by equation (40). The value of  $\epsilon_M$  required in this formula is expressed by equation (34), which cannot be evaluated until equation (40) is evaluated. As a trial value,  $\epsilon_M$  will be assumed equal to 1.0. The drag reduction due to heating is then, by equation (40)

$$\Delta C_D = -\frac{JH\epsilon_H\epsilon_M}{q_0 F V_0} = -\frac{778 \times 68.2 \times 0.0565 \times 1.0}{441 \times 1.009 \times 669} = -0.0101$$

The value of the net force is, finally,

$$C_D = C_{D'} + \Delta C_D = 0.0081 - 0.0101 = -0.0020$$

If this first approximation is used for the net force, a value for  $\epsilon_M$  may be computed from equation (34); that is,

$$\epsilon_M = \frac{1}{1 - \left( \frac{-0.0020 + 0.0081}{4 \times 0.0401} \right)} = 1.04$$

With this value for  $\epsilon_M$ , the new value obtained for the thrust due to heating is

$$\Delta C_D = -0.0101 \times 1.04 = -0.0105$$

and the net force is

$$C_D = 0.0081 - 0.0105 = -0.0024$$

No further trials need be made in this example because  $\epsilon_M$  is so close to unity. The measured value of the net internal drag for this test condition was  $-0.0022$ . The slight difference between the measured and the computed results indicates the small error involved in the assumption of uniform outlet-velocity distribution. The foregoing method is exact except for this assumption.

Comparison of subsonic ram-jet propulsion system with internal-combustion engine.—The compression ratio corresponding to stagnation pressure in the duct at a Mach number of 1.0 is smaller than the values employed in internal-combustion engines. The ideal heat-cycle efficiency for the duct system considered in this report (ram jet) is, therefore, lower at subsonic speeds than for the internal-combustion engine. A number of energy losses, however, occur in the use of the internal-combustion engine that do not occur in the heated duct flow. These losses may be listed as follows:

1. Mechanical losses in the moving parts of the engine
2. Power required for cooling-air flow
3. Increase in airplane drag due to the engine installation
4. Friction and compressibility losses in the propeller

From a consideration of these factors, a value of 24 percent for the thermal efficiency of a typical engine installation was arrived at. This value does not include the induced losses in the propeller slipstream or the compressibility losses. In the case of the duct flow, the present results indicate that the ideal thermal efficiency can be closely approached if the ducting losses can be kept low. Furthermore, the results of references 4, 5, and 7 show that installation of the duct with suitable inlet and outlet openings can be accomplished without increasing the airplane drag. A comparison of the two systems of propulsion is shown in figure 20. The ideal efficiency of the duct system becomes of comparable magnitude to the thermal efficiency of the engine installation at Mach numbers approaching 1.0.

The power recoverable from the cylinder-cooling flow ("Meredith effect," reference 1) in a typical air-cooled engine is also shown in figure 20. The pressure-drop results given in figure 6 were used to compute the compression ratio. The heat to be dissipated in cylinder cooling was assumed to be 0.4 brake horsepower. As shown in the figure, at a given Mach number, greater recovery is possible at sea level than at altitude because the required  $\Delta p/q_0$  increases rapidly with increase in altitude. The energy

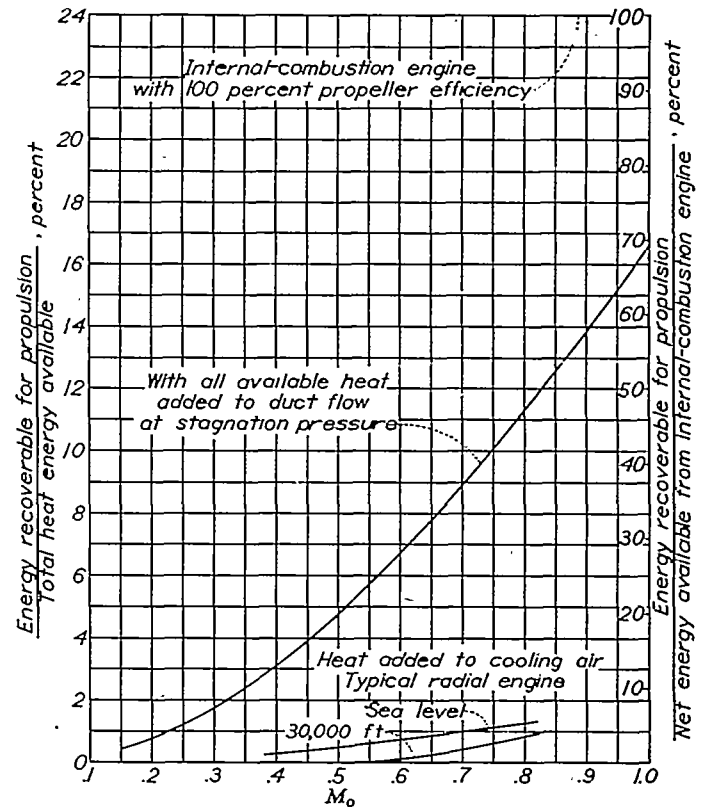


FIGURE 20.—Comparison of the over-all efficiency when the available heat is added in an internal-combustion engine and in the duct at stagnation pressure.

recovery for this air-cooled engine installation thus amounts to about 3 percent of the brake horsepower at sea level at  $M_0=0.60$ , but at 30,000 feet there would be no recovery at this speed. For lower speeds at 30,000 feet the effect of the heat would cause a power loss.

## SUMMARY OF RESULTS

### COMPRESSIBILITY EFFECTS

The results of both the analytical and experimental parts of this investigation are summarized as follows:

1. Compression of the air in the duct ahead of the radiator results in large increases in pressure, temperature, and density at the flight Mach numbers now commonly attained.

2. The Mach number of the flow in the radiator is an important parameter governing the flow changes across the radiator or air-cooled engine. At high internal Mach numbers, the density decrease through the radiator due to the heat added is greatly augmented by the effects of friction and momentum change.

3. A large increase in the pressure drop, corresponding to this density decrease, occurs for a given mass flow as the Mach number advances. This increased pressure drop results partly from increased friction losses and partly from the change in momentum of the air flow within the radiator. The magnitudes of these compressibility or density-change effects increase with radiator drag coefficient as well as with the Mach number.

4. In order to maintain required cooling of air-cooled engines as the altitude is increased, an increasing volume rate of air flow is required because of the reduction in atmospheric density. The Mach number of the internal flow

therefore increases with altitude and the compressibility effects consequently become more severe. It appears that the use of a blower to produce adequate pressure drops at high altitudes will be required for some existing engines.

5. The maximum possible mass-flow rate is attained when sonic velocity is reached at any station in the internal flow system. Increasing the pressure drop after this limiting condition is reached will not increase the mass-flow rate; the added energy will be dissipated in internal shock waves.

6. The attainment of sonic velocity is the limiting possible flow condition regardless of the rate of heating or the magnitude of the internal-friction losses. Increases in either of these factors, however, reduce the mass-flow rate obtained at the limiting flow condition.

7. In conventional cooling-system arrangements, sonic velocity would first be obtained either within the radiator at the tube exits or at the outlet opening. Existing air-cooled engines generally employ much higher cooling-air velocities than an efficient radiator, and the critical flow condition might occur under flight conditions now attainable. Calculations for a typical air-cooled-engine installation indicated that sonic velocity would be attained in the baffle exits at altitudes ranging from about 40,000 to 45,000 feet if a maximum head temperature of 450° F and a fuel-air ratio of 0.10 were maintained.

#### EFFECTS OF HEATING

1. In usual internal flow systems heat is added in an expanded section of the duct where the static pressure is greater than atmospheric pressure. Under these conditions the momentum and the kinetic energy of the flow in the wake are increased. The ratio of the increased kinetic energy to the heat energy added is denoted as the efficiency of the energy-recovery process. The momentum increase, which determines the thrust or drag reduction due to heating, is related to the kinetic-energy gain by a factor depending on the relative magnitudes of the wake velocity and the flight speed.

2. The thermal efficiency of the recovery process depends mainly on the ratio of the static pressure in the duct at the entrance to the heating chamber to the atmospheric pressure and, to a lesser extent, on the Mach number of the flow in the duct, and on the rate of heating. Increases in either the Mach number of the duct flow or the heating rate cause decreases in the efficiency.

3. An important effect of addition of heat in a constant-area duct is to increase the Mach number of the flow. For heating rates corresponding to temperature rises of the order of 2500° F, a Mach number of 1.0 is reached at the end of the duct for an inlet Mach number of about 0.2. This critical or choking inlet Mach number dictates the area expansion required in the diffuser ahead of the combustion chamber.

4. The compression ratio, and hence the efficiency, increases approximately as the square of the flight Mach number. Maximum recovery at a given flight Mach number requires that factors tending to reduce the compression ratio be minimized. Poor installations having large internal-pressure drops will suffer also from decreased gain from the heat-recovery process.

5. The power recoverable from the heat added to the cooling air (Meredith effect) was found to be about 3 percent of the brake horsepower for an existing air-cooled engine at a flight Mach number of 0.60 at sea level. At 30,000 feet, however, no recovery occurred at this flight Mach number, and at lower Mach numbers the recovery was negative.

6. The addition of heat in an internal flow system has a throttling effect on the mass-flow rate. The flow for a given outlet area decreases approximately in proportion to the square root of the outlet density. It is essential that this effect be allowed for in computing the required outlet-opening size.

7. The outlet dynamic pressure  $\frac{1}{2} \rho_4 v_4^2$  does not change appreciably with heating because, in most cases, the reduction in density is nearly offset by an increase in the outlet velocity term  $v_4^2$ . The drag of bodies in the wake, therefore, would not be changed due to heating, except for possible scale effects associated with the reduced Reynolds number in the heated flow.

#### CHARTS AND EQUATIONS

For convenience, the formulas and charts showing the principal heating and compressibility effects are listed as follows:

(a) Pressure, density, and temperature ahead of radiator: figures 2, 3, and 4, and equation (5)

(b) Density decrease within the radiator and across the radiator: figure 5

(c) Pressure drop within the radiator: equation (11) with the aid of figure 5

(d) Pressure drop across radiator: equation (13) or (14) with the aid of figure 2 and figure 5

(e) Effect of density change across radiator on the pressure drop: equation (14)

(f) Temperature rise across radiator: equation (18)

(g) Required outlet area: equation (28) with the mass-flow ratio given by equation (26) or (27) or by figure 7

(h) Ideal efficiency of heat-recovery cycle: equation (35) or (37) or figure 8

(i) Thrust due to the addition of heat: equation (40)

(j) Net force due to heated internal flow: equation (41) with the aid of figure 8

#### CONCLUSIONS

1. The flow details in an efficient internal flow system with addition of heat can be computed with good accuracy by the one-dimensional compressible flow relations presented in part I.

2. The actual thermal efficiency obtainable from a ram-jet type of propulsion system is virtually equal to the ideal thermal efficiency. The thrust available from ram-jets can thus be calculated with good accuracy from simple theory if the rate of heat addition to the flow is known accurately.

## APPENDIX A

### CALCULATION OF PRESSURE DROPS REQUIRED FOR COOLING A TYPICAL AIR-COOLED ENGINE AT HIGH ALTITUDES

**Basic experimental data.**—Test data used to establish the basic sea-level air requirement and pressure drop were obtained on a Pratt & Whitney R-2800-27 engine installed in a nacelle in the Langley 16-foot high-speed wind tunnel. The operating condition and the basic data obtained were as follows:

|   |       |
|---|-------|
| Brake horsepower at 2400 rpm (normal rating), assumed constant with altitude..... | 1600  |
| Fuel-air ratio.....   | 0.10  |
| Air temperature, $T_2$  |       |
| °F.....   | 100   |
| °F abs.....   | 560   |
| Maximum head temperature  |       |
| °F.....   | 450   |
| °F abs.....   | 910   |
| Average head temperature  |       |
| °F.....   | 405   |
| °F abs.....   | 865   |
| Mass flow of cooling air  |       |
| slugs/sec.....  | 1.165 |
| lb/sec.....   | 37.5  |
| Pressure drop $\Delta p_r$ , in. of water.....                                    | 15    |
| Frontal area $A_2$ , sq ft.....   | 17    |
| Equivalent leak area ratio $A_r/A_2$ .....  | 0.14  |

**Variation of mass flow of cooling air with altitude.**—The mass flow required to maintain a fixed head temperature depends on a number of variables, but a discussion of the details of the variation with altitude is considered beyond the scope of this paper. A relation currently in use for determining the mass flow will therefore be used without explanation of its derivation. If a supercharged engine with inter-cooler is assumed, this relation for the mass-flow variation is

$$m_{altitude} = m_{sea\ level} \times \frac{(T_{head} - T_2)^{1.5}_{sea\ level}}{(T_{head} - T_2)^{1.5}_{altitude}}$$

The mass-flow calculations will be carried out for values of the flight Mach number  $M_0$  equal to 0.4, 0.6, and 0.8 through the altitude range. As pointed out in part I, the temperature ahead of the engine  $T_2$  depends on the flight speed as well as on the atmospheric temperature. For Army Summer Air, the value of  $T_2$  was determined from figure 4. For  $M_0$  equal to 0.6, the mass flows computed at altitude by the foregoing relation are as follows:

| Altitude<br>(ft) | $T_0$<br>(°F abs.) | $T_2$<br>(°F abs.) | Mass flow<br>(lb/sec) |
|------------------|--------------------|--------------------|-----------------------|
| 0                | 560                | 600                | 46.3                  |
| 10,000           | 524                | 562                | 38.0                  |
| 20,000           | 489                | 524                | 31.7                  |
| 30,000           | 463                | 486                | 27.0                  |
| 40,000           | 418                | 448                | 23.4                  |
| 50,000           | 400                | 429                | 21.9                  |

The importance of allowing for the temperature rise caused by adiabatic compression ahead of the engine is illustrated by the sea-level case for which the mass flow was only 37.5 pounds per second, the compression effect being neglected, as compared with 46.3 pounds per second shown in the table.

**Details of the pressure-drop calculations.**—The required pressure drop will be computed as the drop between stations 2 and  $r_2$  plus the drop in the baffles. If equation (13) is to be applied to an air-cooled cylinder on which the baffling covers only the rear half of the cylinder, account must be taken of the fact that approximately half of the heat is added to the cooling air ahead of the baffle at virtually constant pressure. Thus, the density of the air immediately ahead of the baffle at station  $2a$  is obtained from the relation

$$\frac{\rho_2}{\rho_{2a}} = 1 + \frac{H/2}{c_p g m T_2}$$

The value of  $H$ , the heat added to the cooling air, was taken as the heat equivalent of 0.4 brake horsepower. Thus, equation (13) for the air-cooled engines becomes

$$\frac{\Delta p_r}{q_2} = \frac{1.43}{M_2^2} \left(1 - \frac{p_{r_2}}{p_2}\right) + \frac{\rho_{2a}}{\rho_2} \left(\frac{A_2}{A_{r_2}}\right)^2 \left[ C_{D_f} + 2 \left(\frac{\rho_{r_2}}{\rho_2} - 1\right) \right]$$

in which  $p_{r_2}/p_2$  and  $\rho_{2a}/\rho_2$  are obtained from figures 2 and 3, respectively, for the design values of  $M_{r_2}$  and  $A_{r_2}/A_2$ .

The ratio  $\rho_{r_2}/\rho_2$  is obtained directly from figure 5 for the design values of  $M_{r_2}$  and  $C_{D_f}$ . The friction component of the engine drag  $C_{D_f}$  is assumed to result only from friction within the baffles and was obtained from the basic engine data as follows:

(1) The over-all test pressure drop  $\Delta p_r$  was 78 lb/sq ft and  $\rho_{2a}/\rho_2$  was 1.08.

(2) Substituting these values in equation (14) gives

$$78 = \Delta p_{r_t} \times \frac{1}{2} (1 + 1.08) + 2 \times 1.07 \times 51 (1.08 - 1) + 1.07 (51 - 1)$$

or

$$\Delta p_{r_t} = 15.2 \text{ lb/sq ft}$$

$$(3) \quad (C_{D_r})_{friction} = \frac{\Delta p_{r_t}}{q_2} = \frac{15.2}{1.07} = 14.2$$

(4) By equation (8),

$$C_{D_f} = \frac{14.2}{2} \times \frac{q_2}{q_{r_2}} \left(1 + \frac{\rho_{r_2}}{\rho_2}\right)$$

As an example, the results of the calculations for a typical flight speed and altitude are listed in the following table:

[Altitude 35,000 ft;  $M_0=0.60$ ]

| Station<br>(See<br>fig. 1.) | $\frac{p}{\text{sq ft}}$ | $\frac{\rho}{\text{cu ft}}$ | $T$<br>(° F) | $M$   | $\frac{q}{\text{sq ft}}$ |
|-----------------------------|--------------------------|-----------------------------|--------------|-------|--------------------------|
| 0                           | 497                      | 0.000666                    | 435          | 0.60  | 125                      |
| 2                           | 630                      | .000788                     | 466          | .0545 | 1.31                     |
| 2a                          | 630                      | .000730                     | 503          | .0567 | -----                    |
| r <sub>2</sub>              | 548                      | .000637                     | 483          | .456  | 79.5                     |
| r <sub>3</sub>              | 498                      | .000543                     | 514          | .518  | -----                    |

The pressure drop across the engine is

$$\Delta p_r = p_2 - p_{r_3} = 132 \text{ lb/sq ft}$$

See figure 6 for pressure drops for other altitudes.

In order to illustrate the large error involved in the neglect of the effects of the density decrease across the engine, the pressure drop will be computed without regard for these effects. In this case, the usual assumption is

$$\frac{\Delta p_r}{q_2} = \text{Constant with altitude}$$

or

$$\frac{\rho}{\rho_{\text{sea level}}} \times \Delta p_r \times \frac{1}{M^2} = \text{Constant with altitude}$$

whence

$$\begin{aligned} \Delta p_r &= \Delta p_{r_{\text{sea level}}} \left( \frac{M_{\text{altitude}}}{M_{\text{sea level}}} \right)^2 \frac{\rho_{\text{sea level}}}{\rho_{\text{altitude}}} \\ &= 96 \left( \frac{0.78}{1.44} \right)^2 3.32 \\ &= 94 \text{ lb/sq ft} \end{aligned}$$

as compared with the exact value, 132 lb/sq ft. (See fig. 6(b).)

The approximate method (equation (14)) for obtaining the pressure drop across the engine without detailed calculation of the flow within the baffles was found to yield approximately the same results as the foregoing more exact analysis except when the velocity of sound was approached in the baffles. The approximate method gives no indication of the attainment of sonic velocity.

## APPENDIX B

### REDUCTION OF DATA FOR TESTS WITH HEAT ADDITION

#### INTERNAL DRAG

No information on the subject of computing, from wake-survey data, the drag due to heated internal flow at high speeds has been published. The method to be described is applicable to the usual experimental case where the rate of heating and the static and total pressures at the outlet are measured. The momentum relation (equation (21)) is the basis of the calculations. When allowance is made for the nonuniformity of the flow, equation (21) becomes

$$D = \int_{A_1} \rho_4 v_4 (V_0 - v_4) dA$$

or

$$C_D = \frac{2}{F} \int_{A_1} \frac{\rho_4 v_4}{\rho_0 V_0^2} (V_0 - v_4) dA$$

It is convenient to write this relation in the form

$$C_D = \frac{2}{F} \int_{A_1} \left(\frac{\rho_4}{\rho_5}\right)^{1/2} \left(\frac{q_4}{q_0}\right)^{1/2} \left[ \left(\frac{\rho_5}{\rho_0}\right)^{1/2} - \left(\frac{q_5}{q_0}\right)^{1/2} \right] dA \quad (42)$$

If the usual assumption is made that the total pressure at station 5 (where  $p_5 = p_0$ ) is the same as the outlet total pressure, the various terms in this relation may be evaluated as follows: From the isentropic relation,

$$\left(\frac{\rho_4}{\rho_5}\right)^{1/2} = \left(\frac{p_4}{p_0}\right)^{1/2\gamma}$$

and, also,

$$\left(\frac{q_4}{q_0}\right)^{1/2} = \left(\frac{h_4 - p_4}{h_0 - p_0}\right)^{1/2} \left[ \frac{(1+\eta)_0}{(1+\eta)_4} \right]^{1/2}$$

in which the total and static pressures are measured and  $1+\eta$  is the compressibility factor. A more useful formula for  $1+\eta$  than that given in the list of symbols involves the total and static pressures as measured in the wake rather than the wake Mach number. This relation is as follows:

$$1+\eta = 1 + 0.357 \frac{h-p}{p(1+\eta)} + 0.051 \left[ \frac{h-p}{p(1+\eta)} \right]^2 + 0.0018 \left[ \frac{h-p}{p(1+\eta)} \right]^3 \dots \approx 1 + \frac{1}{3} \left( \frac{h-p}{p} \right)$$

Similarly, since  $h_4 = h_5$ ,

$$\left(\frac{q_5}{q_0}\right)^{1/2} = \left(\frac{h_4 - p_0}{h_0 - p_0}\right)^{1/2} \left[ \frac{(1+\eta)_0}{(1+\eta)_5} \right]^{1/2}$$

The only remaining term required for the evaluation of equation (42) is  $(\rho_5/\rho_0)^{1/2}$ . The wake density ratio  $\rho_5/\rho_0$

depends on two factors: (1) the rate at which heat is added to the internal flow; and (2) the amount of aerodynamic heating, which in turn is governed by the Mach number  $M_0$  and by the internal loss. The term  $(\rho_5/\rho_0)^{1/2}$  may be evaluated by writing the energy equation between stations 0 and 5.

$$\frac{p_0}{\rho_0} + \frac{V_0^2}{2} + Jg_c T_0 + \frac{JH}{m} = \frac{p_5}{\rho_5} + \frac{v_5^2}{2} + Jg_c T_5$$

If the relations  $p_5 = p_0$ ,  $T_0 = T_5(\rho_5/\rho_0)$ ,  $p_0 = \rho_0 g R T_0$ ,  $c_p = \frac{R}{J(\gamma-1)}$ ,

and  $M_0^2 = \frac{\rho_0 V_0^2}{\gamma p_0}$  are substituted in this equation, then

$$\frac{\rho_5}{\rho_0} = 1 + \frac{\gamma-1}{2} M_0^2 \left( 1 - \frac{q_5}{q_0} \frac{\rho_0}{\rho_5} \right) + \frac{H}{c_p g m T_0}$$

whence,

$$\left(\frac{\rho_5}{\rho_0}\right)^{1/2} = \left[ \frac{1 + 0.20 M_0^2 (q_5/q_0)}{1 + 0.20 M_0^2 + \frac{H}{c_p g m T_0}} \right]^{1/2}$$

These relations for  $(\rho_4/\rho_5)^{1/2}$ ,  $(q_4/q_0)^{1/2}$ ,  $(q_5/q_0)^{1/2}$ , and  $(\rho_5/\rho_0)^{1/2}$ , when substituted into equation (42), determine the internal drag corresponding to the point in the wake at which the pressures are measured. Integration across the outlet opening gives the required value of the total drag coefficient due to the internal flow.

#### EXTERNAL DRAG

The equations for the internal drag apply for the external drag with the following changes:

$$(1) \quad \left(\frac{\rho_5}{\rho_0}\right)^{1/2} = \left[ \frac{1 + 0.20 M_0^2 (q_5/q_0)}{1 + 0.20 M_0^2} \right]^{1/2}$$

(2) The integral (equation (42)) is evaluated between the surface of the model and the outer extremity of the wake.

#### INTERNAL MASS-FLOW COEFFICIENT

$$C = \frac{\rho_4 Q_4}{\rho_0 F V_0} = \frac{1}{F} \int_{A_1} \left(\frac{\rho_4}{\rho_0}\right) \frac{v_4}{V_0} dA = \frac{1}{F} \int_{A_1} \left(\frac{\rho_4}{\rho_5}\right)^{1/2} \left(\frac{\rho_5}{\rho_0}\right)^{1/2} \left(\frac{q_4}{q_0}\right)^{1/2} dA \quad (43)$$

These are the same quantities as already derived in connection with the internal drag coefficient.

#### CALCULATION OF HEAT-CYCLE EFFICIENCY

The heat-cycle efficiency (equation (31)) can be very conveniently computed from the difference between the drag coefficient for the cold condition and the drag coefficient for

the heated condition. From equations (33) and (34),

$$\begin{aligned} \epsilon_H &= \frac{\epsilon_T}{\epsilon_M} = \frac{(D' - D)V_0}{JH\epsilon_M} = \frac{q_0 F V_0}{JH} \left( \frac{C_D' - C_D}{\epsilon_M} \right) \\ &= \frac{q_0 F V_0}{JH} \left\{ (C_D' - C_D) \left[ 1 - \frac{(C_D' + C_D)}{4C} \right] \right\} \end{aligned} \quad (44)$$

Inasmuch as the mass flow is less for the heated condition than for the cold condition, the measured internal drag without heat is therefore greater than the desired value  $D'$  which would be measured if the mass flow did not change. For small variations in mass flow, however, it is possible to correct accurately the drag for the measured unheated condition to the hypothetical unheated condition. The relation between the total-pressure loss for the desired unheated condition and for the measured unheated condition is

$$\left( \frac{\Delta h}{q_0} \right)' = \left( \frac{\Delta h}{q_0} \right)_c \left( \frac{C}{C_c} \right)^2$$

The outlet total pressure for the desired condition is, then,

$$h_4 = h_0 - \left( \frac{\Delta h}{q_0} \right)' q_0$$

With this value for  $h_4$ , the desired value of  $C_D'$  is computed

directly from equation (42). This value of  $C_D'$  permits computation of  $\epsilon_H$  from equation (44).

Equation (44) may be used to evaluate  $\epsilon_H$  either for the wake-survey values of  $C_D$  and  $C_D'$  or for the force-test values of these drag coefficients.

#### REFERENCES

1. Meredith, F. W.: Note on the Cooling of Aircraft Engines with Special Reference to Ethylene Glycol Radiators Enclosed in Ducts. R. & M. No. 1683, British A. R. C., 1936.
2. Winter, H.: Contribution to the Theory of the Heated Duct Radiator. NACA TM No. 893, 1939.
3. Weise, A.: The Conversion of Energy in a Radiator. NACA TM No. 869, 1938.
4. Becker, John V.: Wind-Tunnel Tests of Air Inlet and Outlet Openings on a Streamline Body. NACA ACR, Nov. 1940.
5. Becker, John V., and Baals, Donald D.: High-Speed Tests of a Ducted Body with Various Air-Outlet Openings. NACA ACR, May 1942.
6. Patterson, G. N.: Modern Diffuser Design. The Efficient Transformation of Kinetic Energy to Pressure. Aircraft Engineering, vol. X, no. 115, Sept. 1938, pp. 267-273.
7. Becker, John V., and Baals, Donald D.: Wind-Tunnel Tests of a Submerged-Engine Fuselage Design. NACA ACR, Oct. 1940.
8. Rubert, Kennedy F., and Knopf, George S.: A Method for the Design of Cooling Systems for Aircraft Power-Plant Installations. NACA ARR, March 1942.